

A Constraint Embedding Approach for Dynamics Modeling of Parallel Kinematic Manipulators with Hybrid Limbs

Andreas Müller

Johannes Kepler University, Linz, Austria
a.mueller@jku.at

ABSTRACT

Parallel kinematic manipulators (PKM) are characterized by closed kinematic loops, due to the parallel arrangement of limbs but also due to the existence of kinematic loops within the limbs. Moreover, many PKM are built with limbs constructed by serially combining kinematic loops. Such limbs are called *hybrid*, which form a particular class of complex limbs. Design and model-based control requires accurate dynamic PKM models desirably without model simplifications. Dynamics modeling then necessitates kinematic relations of all members of the PKM, in contrast to the standard kinematics modeling of PKM, where only the forward and inverse kinematics solution for the manipulator (relating input and output motions) are computed. This becomes more involved for PKM with hybrid limbs. In this paper a modular modeling approach is employed, where limbs are treated separately, and the individual dynamic equations of motions (EOM) are subsequently assembled to the overall model. Key to the kinematic modeling is the constraint resolution for the individual loops within the limbs. This local constraint resolution is a special case of the general *constraint embedding* technique. The proposed method finally allows for a systematic modeling of general PKM. The method is demonstrated for the IRSBot-2, where each limb comprises two independent loops.

Keywords– Parallel kinematic manipulator (PKM), complex limbs, kinematic loop, constraints, constraint embedding, redundancy, inverse kinematics, singularity, dynamics, multibody system, model-based control, screws, Lie group $SE(3)$

1 Introduction

Control and design of parallel kinematic manipulators (PKM) for highly dynamic applications necessitate dynamic models with high fidelity as well as computational efficiency. Computationally efficient modeling approaches exist for serial manipulators [1, 2, 3] including recursive $O(n)$ -formulations [4, 5, 6, 7]. PKM are multibody systems (MBS) featuring multiple kinematic loops. The dynamics modeling of such MBS has been advanced in the last four decades, and lead to several established modeling approaches. As far as rigid body MBS (including discrete elastic elements), the latter include formulations in absolute coordinates [8], relative coordinates [2, 9], and natural coordinates [10, 11], which are applicable to general MBS. PKM, on the other hand, possess a particular kinematic topology, which can be exploited for deriving dedicated dynamics models. The majority of PKM are fully parallel, i.e. the moving platform is connected to the ground (fixed platform) by several serial limbs each comprising one actuator. The limbs can topologically be classified as simple and complex. The prevailing class of PKM consists of fully parallel manipulators with *simple limbs*, i.e. each limb is a serial kinematic chain. For such PKM, tailored modeling approaches were presented in a series of publications [12, 13, 14, 15, 16, 17, 18, 19, 20, 21, 22]. The key concept common to these approaches is to model each limb as a kinematic chain with the platform attached, and to use the inverse kinematics solution of the individual limbs to express the overall kinematics and dynamics equations of motions (EOM) in terms of task space coordinates.

PKM with complex limbs form another practically relevant class, for which the Delta robot is a good example. Also gravity compensated PKM often comprise multiple loops [23]. Most complex limbs are built by a serial arrangement of kinematic loops, which are referred to as *hybrid limbs* (occasionally called *serial-parallel limbs*). Moreover, PKM with hybrid limbs constitute another prevailing class of PKM. The systematic modeling of such PKM was reported in [24] as continuation of formulations presented in [25, 22, 26, 27]. The crucial step of this method is the solution of the closure constraints for the kinematic loops within a limb, which are called *intra-limb constraints*. Incorporating this solution, the kinematics and dynamics modeling approach for PKM with simple limbs can be adopted. The loops within a hybrid limb are topologically

independent, and the intra-limb constraints can thus be solved independently. This method of incorporating solutions of loop constraints is referred to as *constraint embedding* [28,29,30]. The embedding technique is well-known in MBS dynamics [31,8,32], where it usually refers to incorporating the solution of velocity and acceleration constraints so to obtain a model in terms of independent generalized velocities and accelerations, which goes back at least to Voronets [33]. A proper constraint embedding further involves the solution of geometric constraints. Solving constraints in closed form, i.e. an 'explicit' constraint embedding, is in general not possible, however. In this paper, a numerical constraint embedding technique for hybrid limbs is presented, complementing the formulation in [24].

The constraint embedding does not involve simplifications, and the model accounts for the dynamics of all bodies. Simplifications were used in various publications, where the loops within limbs are treated as so-called compound joints. To this end, the loop is replaced by an equivalent kinematic transformation. For example, parallelogram loops, which are frequently used to construct complex limbs [34,35,36,37,38], are often modeled by so-called 1-DOF Π -joints [3]. While this is kinematically equivalent (but it should be noticed that possible internal singularities are hidden), it does not account for the dynamics of all members of the substituted loop. The 3-DOF Delta robot is a prominent example where each limb is frequently regarded as a hinged parallelogram Π -joint. The dynamic effect of the parallelogram is either disregarded, or is represented by a lumped mass, as this is formed by slender rods. This does not allow to represent non-symmetric mass distributions or compute joint reactions, however.

The contribution of this paper can be summarized by means of the example in Fig. 1, which shows the 2-DOF IRSBot-2 with two limbs [39]. The kinematics of either limb is to be described in terms of the platform position. This involves two steps: 1) the local solution of the intra-limb loop constraints, and 2) the separate solution of the inverse kinematics problem of the individual limbs. Each limb comprises two loops, and each of the corresponding intra-limb loop constraints can be solved numerically in terms of independent coordinates. These solutions render the limb a serial kinematic chain described by some independent coordinates. The inverse kinematics of the limb, represented as serial chain in terms of the independent coordinates, can now be solved numerically. Compared to the standard MBS approach, this method has a reduced complexity and increased robustness w.r.t. redundant constraints. Standard MBS formulations, on the other hand, do not take into account the specific topology of PKM, and operate on the overall system of constraints. As a consequence, a large system of constraints is to be handled, and often the MBS model involves redundant constraints (e.g. for lower mobility PKM), although the intra-limb constraints are non-redundant, which drastically increases the computational effort. The proposed constraint embedding method treats the intra-limb constraints separately. It thus reduces the system size but also allows handling redundant intra-limb constraints. The proposed local constraint embedding approach implements the two above mentioned steps.

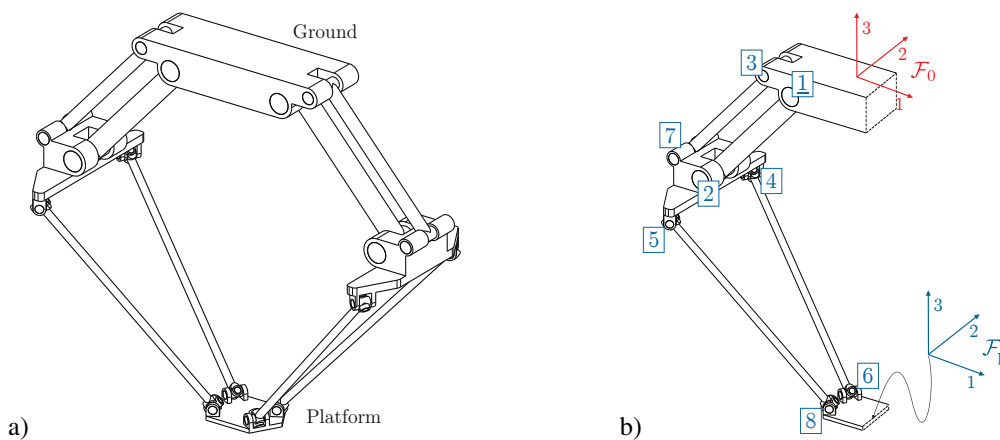


Fig. 1. a) Drawing of the 2-DOF IRSBot-2, whose EE performs pure translations in the 1-3-plane of \mathcal{F}_0 . b) Separated limb comprising two loops with platform frame \mathcal{F}_P assigned.

The paper is organized as follows. In sec. 2, the representation of the kinematic topology of a PKM by means of a linear graph is recalled. Sec. 3 addresses the PKM kinematics, which involves the forward and inverse kinematics of the limbs. A model for the limb kinematics is presented, which involves solutions of the intra-limb loop constraints. The constraint embedding approach is then introduced in sec. 4 as a numerical algorithm for evaluating the constraint solutions. An algorithm for solving the constraints along with the limb inverse kinematics is introduced. The dynamics EOM are presented in sec. 5. The proposed task space formulation builds upon the limb inverse kinematics. Application of the method is presented in detail in sec. 6 for the IRSBot-2 example. The paper closes with a short summary and conclusion in sec. 7. As the cut-joint constraints for technical joints are crucial for PKM modeling, their formulation is summarized in detail in

appendix A. This shall serve as a reference for modeling general robots with kinematic loops. For better readability, a list of symbols is presented in appendix B.

A note on the formalism used for kinematics modeling seems in order: Throughout the paper, the kinematics is described using the Lie group / screw theory formalism, which is a compact and 'user friendly' approach to robot modeling [40,41,42]. However, all relations can be formulated by means of any other modeling approach the reader may prefer.

2 Graph Representation of PKM Topology

The kinematic topology of a PKM is represented by the *topological graph*, a labeled graph denoted Γ [43,44,2]. Bodies are represented by the vertices, and joints by the edges of Γ . The topologically independent loops of Γ are called fundamental cycles (FC). The number of FC is denoted with γ . Fig. 2a) shows the topological graph of a the IRSBot-2 in fig. 1.

Each limb of the PKM connects the base (ground, fixed platform) with the moving platform. Otherwise the limbs are mutually disconnected, and each limb is topologically represented by a subgraph. The subgraph associated to limb l is denoted with $\Gamma_{(l)}$. Vertices (bodies) of $\Gamma_{(l)}$ are numbered with $i = 0, 1, 2, \dots, n_l$, where the ground is indexed with 0. It will be helpful to label the platform with P. Edges (joints) are indexed with $i = 1, \dots, \mathfrak{N}_l$. Fig. 2b) shows the subgraph for a limb of the IRSBot-2. Clearly, all limbs are structurally identical, and thus all $\Gamma_{(l)}$ are congruent.

The peculiarity of complex limbs is that the subgraphs $\Gamma_{(l)}$ possess closed loops, and a set of γ_l FCs can be introduced on $\Gamma_{(l)}$. These FCs are denoted with $\Lambda_{\lambda(l)}, \lambda = 1, \dots, \gamma_l$.

In almost all PKM with complex limbs, the FCs $\Lambda_{(l)}$ within a limb have at most one body in common ($\Lambda_{(l)}$ are edge-disjoint). Such limbs are called *hybrid*, as they can be regarded as serial connection of the kinematic loops. Throughout the paper, the PKM are assumed to possess hybrid limbs only.

A spanning tree on $\Gamma_{(l)}$, denoted $G_{(l)}$, is obtained by removing one edge (called *cut-edge*) of each FC. This defines a tree-topology system comprising n_l moving bodies and n_l joints (tree-edges). From any vertex (body) to the root (ground with index 0) there is a unique path in $G_{(l)}$. A *ground-directed spanning tree* $\vec{G}_{(l)}$ is then introduced by directing all edges of $G_{(l)}$ so to point toward the ground within this path (Fig. 2c). In the so constructed $\vec{G}_{(l)}$, there is a unique directed path from any vertex (moving body) to the ground. In particular, there is a path from platform to ground, and the platform motion is determined by the motion of the corresponding kinematic chain. The latter must indeed respect the loop constraints imposed by the kinematic loops. This induces an ordering, where $j \prec_l i$ denotes that body j is contained in the path from body i to the ground. Edges of $\Gamma_{(l)}$ represent joints with general DOF, but are often used to represent 1-DOF joints, which are used to model multi-DOF joints. Edges of $G_{(l)}$ are called *tree-joints*. The total number of tree-joint variables of limb l is denoted with $n_l \geq \mathfrak{N}_l$. In the following, a canonical numbering is assumed [44,9], i.e. $j \prec_l i$ implies $j < i$.

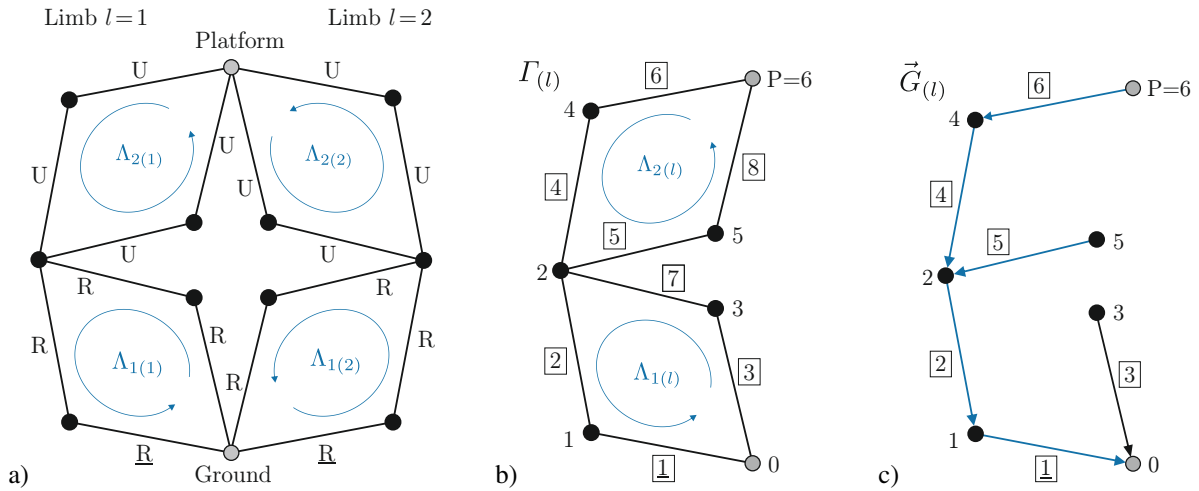


Fig. 2. a) Topological graph Γ of the IRSBot-2. Indicated are the FCs $\Lambda_{1(l)}$ and $\Lambda_{2(l)}$ of the two limbs $l = 1, 2$. b) Subgraph $\Gamma_{(l)}$ of Γ representing limb $l = 1, 2$ of the IRSBot-2. c) A ground-directed spanning tree $\vec{G}_{(l)}$ on $\Gamma_{(l)}$.

3 Kinematics of a Limb

The kinematics of the PKM is completely described by separately describing the kinematics of each limb with the platform attached. In the following, the limbs are regarded separated, i.e. the platform is only connected to one limb, as in fig. 2b) and c).

3.1 Kinematics of Tree-Topology Limbs

The tree-joints determine the configurations of all bodies, including the platform (they are indeed subjected to the closure constraints). The tree-system comprises n_l bodies and joints. The motion of the n_l joints is parameterized by n_l joint variables, which are summarized in the vector $\boldsymbol{\vartheta}_{(l)} := (\vartheta_{1(l)}, \dots, \vartheta_{n_l(l)})^T \in \mathbb{V}^{n_l}$ (subscript (l) indicates limb l). If all joints have 1 DOF, then $n_l = n_l$, but generally, $n_l \geq n_l$. For instance, with the directed tree in fig. 2b), the motion of body 5 of the IRSBot-2 is determined by the joints 1,2, and 5; the platform motion is determined by joints 1,2,4, and 6. The vector of $n_l = 9$ tree-joint variables of limb l is $\boldsymbol{\vartheta}_{(l)} := (\vartheta_{1(l)}, \dots, \vartheta_{9(l)})^T = (\varphi_1, \varphi_2, \varphi_3, \varphi_{4,1}, \varphi_{4,2}, \varphi_{5,1}, \varphi_{5,2}, \varphi_{6,1}, \varphi_{6,2})^T$ where, $\varphi_1, \varphi_2, \varphi_3$ are the three revolute joint angles, and $\varphi_{i,1}, \varphi_{i,2}, i = 4, 5, 6$ are the angles assigned to the three universal joints.

The pose of body k of limb l , i.e. of a body-fixed frame $\mathcal{F}_{k(l)}$, is represented by the homogenous transformation matrix $\mathbf{C}_{k(l)} \in SE(3)$ transforming from $\mathcal{F}_{k(l)}$ to the inertial frame (IFR) \mathcal{F}_0 . Denote with $\mathbf{Y}_i, i = 1, \dots, n_l$ the screw coordinate vector associated to the joint variable i , represented in the IFR. Then the pose of body k is determined by

$$\mathbf{C}_{k(l)}(\boldsymbol{\vartheta}_{(l)}) = f_{k(l)}(\boldsymbol{\vartheta}_{(l)})\mathbf{A}_{k(l)} \quad (1)$$

with the product of exponentials [45, 40, 46] (omitting subscript (l))

$$f_k(\boldsymbol{\vartheta}) = \exp(\vartheta_{\underline{k}}\mathbf{Y}_{\underline{k}}) \cdots \exp(\vartheta_{k-1}\mathbf{Y}_{k-1}) \exp(\vartheta_k\mathbf{Y}_k) \quad (2)$$

where $\mathbf{A}_{k(l)} = \mathbf{C}_{k(l)}(\mathbf{0}) \in SE(3)$ is the zero reference configuration of body k in limb l , and \underline{k} is the index of the last joint in the chain from body k to the ground (with the canonical ordering, body \underline{k} is the predecessor of k with the lowest index). The product of exponentials can also be expressed as

$$f_k(\boldsymbol{\vartheta}) = \mathbf{B}_{\underline{k}} \exp(\vartheta_{\underline{k}}\mathbf{X}_{\underline{k}}) \cdots \mathbf{B}_{k-1} \exp(\vartheta_{k-1}\mathbf{X}_{k-1}) \mathbf{B}_k \exp(\vartheta_k\mathbf{X}_k) \quad (3)$$

where $\mathbf{B}_{k(l)} \in SE(3)$ is the reference configuration of body k relative to its predecessor within limb l , and \mathbf{X}_k is the screw coordinate vector of joint k represented in body-fixed frame at body k . The two forms of the POE are related by $\mathbf{Y}_k = \mathbf{Ad}_{\mathbf{C}_k}\mathbf{X}_k$. The pose of the platform (index P) is thus

$$\mathbf{C}_{p(l)}(\boldsymbol{\vartheta}_{(l)}) = \boldsymbol{\Psi}_{p(l)}(\boldsymbol{\vartheta}_{(l)}) \quad (4)$$

with $\boldsymbol{\Psi}_{p(l)}(\boldsymbol{\vartheta}_{(l)}) := f_{p(l)}(\boldsymbol{\vartheta}_{(l)})\mathbf{A}_p$. Note that the reference configuration of the platform is the same for all limbs.

The body-fixed twist $\mathbf{V}_{k(l)} = (\mathbf{}^k\boldsymbol{\omega}_{k(l)}, \mathbf{}^k\mathbf{v}_{k(l)})^T$ of body k in limb l is determined by the geometric Jacobian as

$$\mathbf{V}_{k(l)} = \mathbf{J}_{k(l)}\dot{\boldsymbol{\vartheta}}_{(l)}. \quad (5)$$

The geometric Jacobian \mathbf{J}_k can be expressed explicitly in terms of the screw coordinate vectors \mathbf{Y}_i or \mathbf{X}_i [24, 40, 47, 41]. It is already available as the block row of the system Jacobian $\mathbf{A}_{(l)}$, as described next.

Denote with $\mathbf{V}_{(l)} := (\mathbf{V}_1, \dots, \mathbf{V}_{n_l}) \in \mathbb{R}^{6n_l}$ the system twist vector of limb l . In terms of the tree-joint rates $\dot{\boldsymbol{\vartheta}}_{(l)}$, this is

$$\mathbf{V}_{(l)} = \mathbf{J}_{(l)}\dot{\boldsymbol{\vartheta}}_{(l)}, \quad \text{with } \mathbf{J}_{(l)} = \begin{pmatrix} \mathbf{J}_{1(l)} \\ \vdots \\ \mathbf{J}_{n_l(l)} \end{pmatrix} \quad (6)$$

with the *geometric system Jacobian* $\mathbf{J}_{(l)}$. The latter factorizes as

$$\mathbf{J}_{(l)} = \mathbf{A}_{(l)}\mathbf{X}_{(l)}. \quad (7)$$

Assuming a canonically directed spanning tree $\vec{G}_{(l)}$, matrix $A_{(l)}(\vartheta)$ is the block-triangular, and $X_{(l)}$ is the block-diagonal

$$A_{(l)} = \begin{pmatrix} \mathbf{I} & \mathbf{0} & \mathbf{0} & \cdots & \mathbf{0} \\ & \mathbf{I} & \mathbf{0} & \cdots & \mathbf{0} \\ & & \ddots & \ddots & \\ & \mathbf{Ad}_{C_{i,j}} & & & \mathbf{0} \\ & & & & \mathbf{I}_{(l)} \end{pmatrix}, X_{(l)} = \begin{pmatrix} {}^1\mathbf{X}_1 & \mathbf{0} & \mathbf{0} & & \mathbf{0} \\ \mathbf{0} & {}^2\mathbf{X}_2 & \mathbf{0} & \cdots & \mathbf{0} \\ \mathbf{0} & \mathbf{0} & {}^3\mathbf{X}_3 & & \mathbf{0} \\ \vdots & \vdots & \ddots & \ddots & \\ \mathbf{0} & \mathbf{0} & \cdots & \mathbf{0} & {}^{n_l}\mathbf{X}_{n_l} \end{pmatrix} \quad (8)$$

where $\mathbf{Ad}_{C_{i,j}} = \mathbf{0}$ if $j \not\prec i$ (body j is not a predecessor of body i).

The time derivative of the Jacobian can be expressed in closed form [24, 47, 48] as

$$\dot{J}(\vartheta, \dot{\vartheta}) = -A(\vartheta) \mathbf{a}(\dot{\vartheta}) J(\vartheta) \quad (9)$$

with $\mathbf{a}(\dot{\vartheta}) := \text{diag}(\dot{\vartheta}_1 \mathbf{ad}_{\mathbf{x}_1}, \dots, \dot{\vartheta}_{n_l} \mathbf{ad}_{\mathbf{x}_{n_l}})$, where $\mathbf{ad}_{\mathbf{x}}\mathbf{Y}$ is the adjoint operator matrix expressing the Lie bracket of two screws. The system acceleration of limb l is thus

$$\dot{V}_{(l)} = J_{(l)} \ddot{\vartheta}_{(l)} + \dot{J}_{(l)} \dot{\vartheta}_{(l)}. \quad (10)$$

Remark 1. *The Lie group formulation has several advantages. Firstly it is important to notice that the kinematic topology enters in the description via the matrix $A_{(l)}$ only. This is common feature of all matrix formulations, which is also represented in the more general setting of spatial operator algebra [29, 44, 9]. Its main advantage, however, is that it combines the classical zero-reference formulation [49] with the coordinate invariant geometric modeling in terms of joint screws [50]. This coordinate invariance admits using the screw coordinates in the reference configuration, likewise represented in the body-fixed or the spatial inertial frame. The kinematic relations is then computationally efficient expressed by the POE (2) or (3) as the exponential on $SE(3)$ admits efficient implementations [51].*

3.2 Task Space Velocity

The constraints imposed by the L limbs determine the mobility of the PKM platform. The platform DOF is denoted $\delta_p \leq 6$. For describing the tasks, δ_p components of the platform twist \mathbf{V}_p are used. These components form the *task space velocity* $\mathbf{V}_t \in \mathbb{R}^{\delta_p}$. The platform twist is usually represented in the platform frame \mathcal{F}_p (collocated with the end-effector), and is aligned so that \mathbf{V}_t consists of exactly δ_p components of the vector \mathbf{V}_p . This is expressed as

$$\mathbf{V}_p = \mathbf{P}_p \mathbf{V}_t \quad (11)$$

with a unimodular $6 \times \delta_p$ velocity distribution matrix \mathbf{P}_p , assigning the δ_p components of the task space velocity to the components of the platform twist. Typical choices for often used task spaces can be found in [24]. If the task velocity allocation changes with the task motion, matrix \mathbf{P}_p will be configuration dependent.

3.3 Loop Constraints within Hybrid Limbs

When limbs separated, only the kinematic loops within the individual limbs remain. Limb l possesses γ_l FCs, denoted $\Lambda_{\lambda(l)}$, $\lambda = 1, \dots, \gamma_l$, and for each FC, a system of loop closure constraints is introduced, referred to as *intra-limb constraints*. The number of constraints imposed by FC $\Lambda_{\lambda(l)}$ is denoted with $m_{\lambda,l}$. It is assumed in the following that these $m_{\lambda,l}$ constraints are independent. Limbs where this is not satisfied are overconstrained, and must be dealt with separately (see remark 3 and 4).

The tree $G_{(l)}$ is obtained by removing one edge from each FC. That is, each FC is cut open, and the joint corresponding to the eliminated edge is called the *cut-joint* of the FC [52]. Loop closure then imposes constraints on the tree-joint variables $\vartheta_{(l)}$ of limb l . More precisely, for hybrid limbs the FC are edge-disjoint, so that loop closure of $\Lambda_{\lambda(l)}$ only constrains the $n_{\lambda,l}$ tree-joint variables belonging to this FC. The latter are denoted with $\vartheta_{(\lambda,l)} \in \mathbb{V}^{n_{\lambda,l}}$. The cut-joint of FC $\Lambda_{\lambda(l)}$ in limb l gives rise to $m_{\lambda,l}$ geometric, velocity, and acceleration constraints of the form

$$\mathbf{g}_{(\lambda,l)}(\vartheta_{(\lambda,l)}) = \mathbf{0} \quad (12)$$

$$\mathbf{G}_{(\lambda,l)} \dot{\vartheta}_{(\lambda,l)} = \mathbf{0} \quad (13)$$

$$\mathbf{G}_{(\lambda,l)} \ddot{\vartheta}_{(\lambda,l)} + \dot{\mathbf{G}}_{(\lambda,l)} \dot{\vartheta}_{(\lambda,l)} = \mathbf{0}. \quad (14)$$

The solution variety of the geometric constraints of $\Lambda_{\lambda(l)}$ is $V_{\lambda,l} := \{\vartheta_{(\lambda,l)} \in \mathbb{V}^{n_{\lambda,l}} | \mathbf{g}_{(\lambda,l)}(\vartheta_{(\lambda,l)}) = \mathbf{0}\}$, which has dimension $\delta_{\lambda,l} = n_{\lambda,l} - m_{\lambda,l}$. The configuration space of the separated hybrid limb l is $V_l := \{\vartheta_{(l)} \in \mathbb{V}^{n_l} | \mathbf{g}_{(\lambda,l)}(\vartheta_{(\lambda,l)}) = \mathbf{0}, \lambda = 1, \dots, \gamma_l\} \subset \mathbb{V}^{n_l}$. Its dimension is denoted with δ_l , which is the DOF of the limb when separated from the PKM.

3.4 Constraint Resolution

The constraints for $\Lambda_{\lambda(l)}$ involve the $n_{\lambda,l}$ coordinates $\vartheta_{(\lambda,l)}$ within this FC only, i.e. $g_{(\lambda,l)}$ depends on $\vartheta_{(\lambda,l)}$ only. Moreover, when the hybrid limb l is connected to the platform only, the constraints can be solved for the γ_l FC independently. This will be referred to as *local constraint embedding*, and is a main step in the proposed modeling approach.

Geometric Constraints: The submersion theorem ensures that the intra-limb constraints (12) possess a local solution $\vartheta_{(\lambda,l)} = \Psi_{(\lambda,l)}(\mathbf{q}_{(\lambda,l)})$ in terms of $\delta_{\lambda,l} := n_{\lambda,l} - m_{\lambda,l}$ independent coordinates $\mathbf{q}_{(\lambda,l)} \in M_{\lambda,l} \subset \mathbb{V}^{\delta_{\lambda,l}}$. The $\mathbf{q}_{(\lambda,l)}$ serve as generalized coordinates with coordinate manifold $M_{\lambda,l}$. The solution, i.e. the map $\Psi_{(\lambda,l)} : M_{\lambda,l} \subset \mathbb{V}^{\delta_{\lambda,l}} \rightarrow V_{\lambda,l} \subset \mathbb{V}^{n_{\lambda,l}}$, can generally not be determined in closed form. A computational method is introduced in sec. 4.1.2 to this end.

There may be $\delta_{0,l}$ joint variables, denoted with $\mathbf{q}_{(0,l)} \in \mathbb{V}^{\delta_{0,l}}$, that are not included in any FC, and thus serve as further independent generalized coordinates. The $\mathbf{q}_{(0,l)}$ along with $\mathbf{q}_{(\lambda,l)}, \lambda = 1, \dots, \gamma_l$ represents the overall set of $\delta_l := \delta_{0,l} + \delta_{1,l} + \dots + \delta_{\gamma_l,l}$ generalized coordinates for the separated hybrid limb, denoted $\mathbf{q}_{(l)}$. The configuration of limb l is thus expressed in terms of δ_l independent coordinates $\mathbf{q}_{(l)} \in M_l \subset \mathbb{V}^{\delta_l}$ with the *solution map*

$$\begin{aligned} \Psi_{(l)} : M_l &\rightarrow V_l \\ \mathbf{q}_{(l)} &\mapsto \vartheta_{(l)} = \Psi_{(l)}(\mathbf{q}_{(l)}) \end{aligned} \quad (15)$$

which summarizes the $\Psi_{(\lambda,l)}, \lambda = 1, \dots, \gamma_l$.

Velocity and Acceleration Constraints: The coordinates are partitioned as $\vartheta_{(\lambda,l)} = (\mathbf{y}_{(\lambda,l)}, \mathbf{q}_{(\lambda,l)})$, where $\mathbf{y}_{(\lambda,l)}$ are the remaining $m_{\lambda,l}$ dependent joint variables in the FC. The constraints (13) can then be written as

$$\mathbf{G}_{\mathbf{y}_{(\lambda,l)}} \dot{\mathbf{y}}_{(\lambda,l)} + \mathbf{G}_{\mathbf{q}_{(\lambda,l)}} \dot{\mathbf{q}}_{(\lambda,l)} = \mathbf{0} \quad (16)$$

with the regular $m_{\lambda,l} \times m_{\lambda,l}$ submatrix $\mathbf{G}_{\mathbf{y}_{(\lambda,l)}}$ and the $m_{\lambda,l} \times \delta_{\lambda,l}$ submatrix $\mathbf{G}_{\mathbf{q}_{(\lambda,l)}}$ corresponding to the dependent joint rates $\dot{\mathbf{y}}_{(\lambda,l)}$ and to the independent joint rates $\dot{\mathbf{q}}_{(\lambda,l)}$, respectively. With the assumed independence of constraints, the constraint Jacobian $\mathbf{G}_{(\lambda,l)}(\vartheta_{(\lambda,l)})$ is a regular $m_{\lambda,l} \times n_{\lambda,l}$ matrix. The solution of velocity and acceleration constraints (13) and (14) are, respectively,

$$\begin{pmatrix} \dot{\mathbf{y}}_{(\lambda,l)} \\ \dot{\mathbf{q}}_{(\lambda,l)} \end{pmatrix} = \mathbf{H}_{(\lambda,l)} \dot{\mathbf{q}}_{(\lambda,l)}, \quad \begin{pmatrix} \ddot{\mathbf{y}}_{(\lambda,l)} \\ \ddot{\mathbf{q}}_{(\lambda,l)} \end{pmatrix} = \mathbf{H}_{(\lambda,l)} \ddot{\mathbf{q}}_{(\lambda,l)} + \dot{\mathbf{H}}_{(\lambda,l)} \dot{\mathbf{q}}_{(\lambda,l)}. \quad (17)$$

The $n_{\lambda,l} \times \delta_{\lambda,l}$ matrix $\mathbf{H}_{(\lambda,l)}$ is an orthogonal complement of $\mathbf{G}_{(\lambda,l)}$. With the partitioning, it and its derivative is explicitly

$$\mathbf{H}_{(\lambda,l)} := \begin{pmatrix} -\mathbf{G}_{\mathbf{y}_{(\lambda,l)}}^{-1} \mathbf{G}_{\mathbf{q}_{(\lambda,l)}} \\ \mathbf{I} \end{pmatrix}_{(\lambda,l)} \quad (18)$$

$$\dot{\mathbf{H}}_{(\lambda,l)}(\vartheta_{(\lambda,l)}, \dot{\vartheta}_{(\lambda,l)}) = \begin{pmatrix} \mathbf{G}_{\mathbf{y}_{(\lambda,l)}}^{-1} (\dot{\mathbf{G}}_{\mathbf{y}_{(\lambda,l)}} \mathbf{G}_{\mathbf{y}_{(\lambda,l)}}^{-1} \mathbf{G}_{\mathbf{q}_{(\lambda,l)}} - \dot{\mathbf{G}}_{\mathbf{q}_{(\lambda,l)}}) \\ \mathbf{0} \end{pmatrix}_{(\lambda,l)}. \quad (19)$$

Combining (17) for all FCs yields the overall solution of the intra-limb constraints

$$\dot{\vartheta}_{(l)} = \mathbf{H}_{(l)} \dot{\mathbf{q}}_{(l)}, \quad \ddot{\vartheta}_{(l)} = \mathbf{H}_{(l)} \ddot{\mathbf{q}}_{(l)} + \dot{\mathbf{H}}_{(l)} \dot{\mathbf{q}}_{(l)}. \quad (20)$$

Remark 2. It should be noticed that $\mathbf{q}_{(\lambda,l)}$ are local coordinates on the solution variety $V_{\lambda,l}$. If the PKM exhibits different motion modes, it may be necessary to switch between coordinates and different $M_{\lambda,l}$ accordingly. Moreover, in case of kinematotropic PKM [53, 54] the DOF δ_l is different in different motion modes.

Remark 3. The selection of independent velocities (coordinates) is not unique. A particular choice of $\mathbf{q}_{(\lambda,l)}$ corresponds to a particular choice of $\mathbf{G}_{\mathbf{y}(\lambda,l)}$. The choice determines the numerical conditioning of the matrix $\mathbf{H}_{(\lambda,l)}$. This problem was addressed in [31, 55, 56], where a generalized coordinate partitioning approach was introduced. Computational aspects were addressed from a geometric perspective in [57, 58, 59]. In general, an orthogonal complement of $\mathbf{G}_{(\lambda,l)}$, and thus $\mathbf{q}_{(\lambda,l)}$, can be determined numerically using SVD or QR decompositions to compute the null-space of $\mathbf{G}_{(\lambda,l)}$. Besides numerical approaches, a solution of the velocity constraints can be obtained with the reciprocal screw approach [3, 24]. This allows for algebraic determination, possibly avoiding matrix inversions.

Remark 4. A problem often encountered, is that of constraint redundancy, i.e. some of the $m_{\lambda,l}$ constraints are dependent, so that the DOF of $\Lambda_{\lambda(l)}$ is $\delta_{\lambda,l} > n_{\lambda,l} - m_{\lambda,l}$, which leads to a singular constraint Jacobian. The FC is then classified as overconstrained. For most PKM with complex limbs, the intra-limb constraints are not redundant (see sec. 4.3). The 3R[2UU] Delta robot is an example where the intra-limb constraints are redundant. (The notation 3R[2UU] indicates that the PKM has three limbs, articulated arm is attached to the base by an actuated R joint, and the arm and platform are connected by two parallel rods with U joints at both ends). A limb contains a single loop with four U joints. The loop constraints are redundant since the axes of the different U joints are parallel.

Remark 5. With the cut-joint formulation, the number of the constraints, and thus the number of tree-joint variable (i.e. the size of the EOM of a limb), depend on the selected cut-joint giving rise to specific cut-joint constraints (see appendix A). The modeling and constraint formulation could be simplified by using the cut-body approach. Then, the loop constraints are simply expressed as $f_{\lambda,l}(\boldsymbol{\vartheta}) = \mathbf{I}$, with

$$f_{\lambda,l}(\boldsymbol{\vartheta}) = \exp(\vartheta_1 \mathbf{Y}_1) \cdots \exp(\vartheta_{N_{\lambda,l}} \mathbf{Y}_{N_{\lambda,l}})$$

where $\vartheta_1, \dots, \vartheta_{N_{\lambda,l}}$ denote the joint angles of all $N_{\lambda,l}$ joints in the FC $\Lambda_{\lambda(l)}$ (including the cut-joint). This, however, always leads to a system of six equations for all $N_{\lambda,l}$ joint variables, and thus to a larger system of constraints and a larger system of EOM. On the other hand, the computation of the constraints is always the same irrespective of the type of joints. This approach is usually followed in mechanism theory, while the cut-joint formulation is exclusively used in MBS dynamics.

3.5 Forward Kinematics of Separated Limb

The forward kinematics problem of limb l is to determine the motion of all bodies in terms of the generalized coordinates $\mathbf{q}_{(l)}$. The configuration of body k of limb l is given in terms of the tree-joint variables by (1), and that of the platform by (4) with the map $\Psi_{p(l)}$. Introducing the solution (15) of the intra-limb constraints, the platform motion as part of the complex limb is given in terms of the generalized coordinates as $\mathbf{C}_{p(l)}(\boldsymbol{\vartheta}_{(l)}) = \Phi_{p(l)}(\mathbf{q}_{(l)})$ with the *forward kinematics map of limb l* , $\Phi_{p(l)} : M_{(l)} \rightarrow W_{(l)}$, defined as

$$\Phi_{p(l)} := \Psi_{p(l)} \circ \Psi_{(l)}. \quad (21)$$

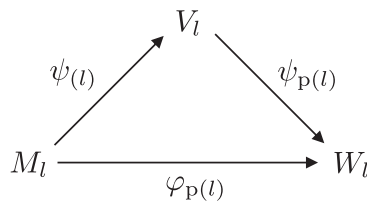
The forward kinematics map is surjective, and the image of $\Phi_{p(l)}$ is the workspace $W_{(l)} \subset SE(3)$ of the separated complex limb. The platform DOF of the separated limb, denoted with $\delta_{p(l)} := \dim W_{(l)}$, is the dimension of the workspace $W_{(l)} = \text{im } \Phi_{p(l)}$ of the limb. As for serial robotic manipulators, a limb can be kinematically redundant. If the DOF of the limb is greater than its platform DOF, $\delta_{p(l)} < \delta_l$, the limb is *structurally redundant*, i.e. the limb can perform finite motions even if the platform is locked.

Combining the constraint solution (20) with the geometric Jacobian (5) of the platform, yields the *forward kinematics Jacobian of limb l*

$$\mathbf{L}_{p(l)} := \mathbf{J}_{p(l)} \mathbf{H}_{(l)} \quad (22)$$

which determines the EE-twist as $\mathbf{V}_{p(l)} = \mathbf{L}_{p(l)} \dot{\mathbf{q}}_{(l)}$. The rank of $\mathbf{L}_{p(l)}$ is $\delta_{p(l)}$.

For deriving the numerical constraint embedding, it will be helpful to represent the forward kinematics relation by the following commutation diagram.



3.6 Inverse Kinematics

The inverse kinematics problem of the PKM mechanism is to determine the motion of all bodies, i.e. the joint angles $\boldsymbol{\vartheta}_{(l)}(t)$, for a given platform motion of the PKM. In the following, the limbs are assumed to be non-redundant, i.e. $\delta_{p(l)} = \delta_l$.

The inverse of $\boldsymbol{\varphi}_{p(l)}$ exists, and $\boldsymbol{\varphi}_{p(l)}^{-1} : W_{(l)} \rightarrow M_{(l)}$ determines the generalized coordinates for given platform pose. For general PKM, also with non-redundant limbs, the solution of the inverse kinematics problem of the limb is not unique, since the map $\boldsymbol{\varphi}_{p(l)}$ is surjective but not bijective, which must be accounted for when solving the inverse kinematics problem numerically.

When all limbs are assembled, the platform must respect the corresponding constraints imposed by all L limbs, thus the workspace of the PKM is $W = \cap_{l=1}^L W_{(l)}$. The DOF of the platform as part of the PKM is $\delta_p = \dim W$. It will be important to distinguish whether the platform DOF of the PKM is lower than the platform DOF of the separated limb. Limb l is called *equimobile* iff $\delta_p = \delta_{p(l)}$ [60, 24], which means that the PKM workspace is an equidimensional subspace of the workspaces of the limbs. The inverse map $\boldsymbol{\varphi}_{p(l)}^{-1}$ restricted to W is called the *inverse kinematics map of limb l* , denoted $f_{(l)} := \boldsymbol{\varphi}_{p(l)}^{-1}|_W$

$$\begin{aligned} f_{(l)} : W &\rightarrow M_{(l)} \\ \mathbf{C}_p &\mapsto \mathbf{q}_{(l)} = f_{(l)}(\mathbf{C}_p) \end{aligned} \quad (23)$$

which assigns to an admissible platform pose of the PKM the generalized coordinates of limb l . Solving the inverse kinematics problem thus boils down to evaluating $f_{(l)}$. This must be performed locally due to the non-uniqueness. The inverse kinematics problem is solved, i.e. the map (23) is evaluated, numerically employing the velocity inverse kinematics.

Consider limb l separated from the PKM but with the platform attached. The platform twist is determined by $\mathbf{V}_{p(l)} = \mathbf{L}_{p(l)}\dot{\mathbf{q}}_{(l)}$, with the Jacobian (22). The platform attached to a separated limb has $\delta_{p(l)}$ DOF, and the forward kinematics Jacobian $\mathbf{L}_{p(l)}$ has rank $\delta_{p(l)}$. Denote with $\mathbf{L}_{t(l)}$ the *task space Jacobian of limb l* defined as the full rank $\delta_{p(l)} \times \delta_l$ submatrix of $\mathbf{L}_{p(l)}$ so that $\mathbf{L}_{t(l)}\dot{\mathbf{q}}_{(l)}$ delivers the $\delta_{p(l)}$ components of the platform velocity when attached to the separated limb, similarly to the forward kinematics Jacobian of a serial robot.

Now consider the PKM with all limbs assembled. For an equimobile limb, the task space velocity \mathbf{V}_t comprises exactly $\delta_{p(l)} = \delta_p$ components of $\mathbf{V}_{p(l)}$, while for a non-equimobile PKM, it only consists of $\delta_p < \delta_{p(l)}$ components (the platform DOF of a separated limb is different from the platform DOF within the PKM). For equimobile limbs, this implies

$$\mathbf{V}_t = \mathbf{L}_{t(l)}\dot{\mathbf{q}}_{(l)}. \quad (24)$$

For non-equimobile limbs, in addition to the $\delta_{p(l)}$ rows of $\mathbf{L}_{t(l)}$ that determine the task velocities, there are $\delta_{p(l)} - \delta_p$ rows of $\mathbf{L}_{t(l)}$ that correspond to the components of the platform twist of the separated limb that must be zero when all limbs are assembled to the PKM. These constraints on the limb along with the forward kinematics are expressed as

$$\mathbf{D}_{t(l)}\mathbf{V}_t = \mathbf{L}_{t(l)}\dot{\mathbf{q}}_{(l)} \quad (25)$$

where $\mathbf{D}_{t(l)}$ is a $\delta_{p(l)} \times \delta_p$ velocity distribution matrix, which assigns the components of the task space velocity \mathbf{V}_t to the relevant rows of the task space Jacobian of limb l . For equimobile limbs, $\mathbf{D}_{t(l)}$ is the identity matrix. The platform DOF of the IRSBot-2, for example, is $\delta_p = \delta = 2$. The platform DOF of a separated limb is $\delta_{p(l)} = 3$, however, so that it is non-equimobile (see sec. 6). Relative to the platform frame \mathcal{F}_p shown in fig. 1, the task space velocity $\mathbf{V}_t = (v_1, v_3)^T$ consists of the 1- and 3-component of the translation velocity, and

$$\mathbf{D}_{t(l)} = \begin{pmatrix} 1 & 0 \\ 0 & 0 \\ 0 & 1 \end{pmatrix}. \quad (26)$$

For non-redundant limbs, $\mathbf{L}_{t(l)}$ is square and invertible. The velocity inverse kinematics solution is thus

$$\dot{\mathbf{q}}_{(l)} = \mathbf{F}_{(l)}\mathbf{V}_t, \quad \text{with } \mathbf{F}_{(l)} = \mathbf{L}_{t(l)}^{-1}\mathbf{D}_{t(l)} \quad (27)$$

where $\mathbf{F}_{(l)}$ is the *inverse kinematics Jacobian of limb l* . With (20), the velocity of all joints of the limb is then

$$\dot{\boldsymbol{\vartheta}}_{(l)} = \mathbf{H}_{(l)}\mathbf{F}_{(l)}\mathbf{V}_t. \quad (28)$$

The joint accelerations are then

$$\begin{aligned}\ddot{\boldsymbol{\vartheta}}_{(l)} &= \mathbf{H}_{(l)}\mathbf{F}_{(l)}\dot{\mathbf{V}}_t + (\dot{\mathbf{H}}_{(l)} - \mathbf{H}_{(l)}\mathbf{F}_{(l)}\dot{\mathbf{L}}_{t(l)})\mathbf{F}_{(l)}\mathbf{V}_t \\ &= \mathbf{H}_{(l)}\mathbf{F}_{(l)}\dot{\mathbf{V}}_t + (\dot{\mathbf{H}}_{(l)} - \mathbf{H}_{(l)}\mathbf{F}_{(l)}\dot{\mathbf{L}}_{t(l)})\dot{\mathbf{q}}_{(l)}\end{aligned}\quad (29)$$

with $\dot{\mathbf{H}}_{(l)}$ in (19), and $\dot{\mathbf{L}}_{p(l)}(\boldsymbol{\vartheta}_{(l)}, \dot{\boldsymbol{\vartheta}}_{(l)}) = \mathbf{J}_{p(l)}\mathbf{H}_{(l)} + \mathbf{J}_{p(l)}\dot{\mathbf{H}}_{(l)}$.

3.7 Inverse Kinematics of PKM

The above kinematics description of individual limbs can be immediately employed to the kinematics modeling of the overall PKM. Denote with $\boldsymbol{\vartheta}_{\text{act}} \in \mathbb{V}^{n_{\text{act}}}$ the n_{act} joint variables of the actuated joints of the PKM. It is assumed that the PKM is fully actuated, i.e. the forward kinematics map $\boldsymbol{\varphi}_{\text{FK}} : \mathbb{V}^{n_{\text{act}}} \rightarrow W$ is well-defined and surjective. It determines the platform motion for given actuator motion, $\mathbf{C}_p = \boldsymbol{\varphi}_{\text{FK}}(\boldsymbol{\vartheta}_{\text{act}})$. If the PKM is non-redundantly actuated ($n_{\text{act}} = \delta$) [61], the actuator coordinates represent generalized coordinates $\mathbf{q} := \boldsymbol{\vartheta}_{\text{act}}$ of the PKM. If it is redundantly actuated ($n_{\text{act}} > \delta$), only δ of them can be used as generalized coordinates.

The inverse kinematics problem of the PKM is to determine the actuator motion for given platform motion. The inverse $f_{\text{IK}} := \boldsymbol{\varphi}_{\text{FK}}^{-1}$ is the *inverse kinematics map of the PKM*, which assigns the actuator coordinates to the platform configuration, $\boldsymbol{\vartheta}_{\text{act}} = f_{\text{IK}}(\mathbf{C}_p)$. This is defined already by the inverse kinematics map f_i in (23) of the individual limbs.

The actuator velocities are also known already from (27). The solution of the velocity inverse kinematics problem is thus

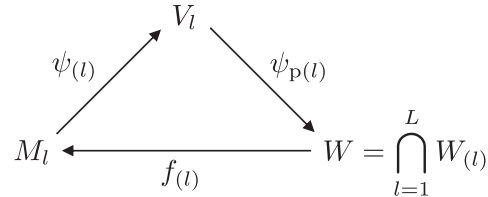
$$\dot{\boldsymbol{\vartheta}}_{\text{act}} = \mathbf{J}_{\text{IK}}\mathbf{V}_t \quad (30)$$

with \mathbf{J}_{IK} being the $n_{\text{act}} \times \delta_p$ *inverse kinematics Jacobian of the PKM*, which consists of the rows of $\mathbf{F}_{(l)}$, $l = 1, \dots, L$ in (27) corresponding to the actuator coordinates.

4 Numerical Constraint Embedding

4.1 Nested Solution Scheme

Local constraint embedding refers to solving the inverse kinematics problem of the limbs, i.e. evaluating the inverse kinematics map $f_{(l)}$ in (23). This involves solving the intra-limb constraints (12), i.e. evaluating $\boldsymbol{\psi}_{(l)}$ in (15). An iterative numerical solution scheme is proposed to this end. Its iterative nature necessitates separate correction steps for the evaluation of $f_{(l)}$ and $\boldsymbol{\psi}_{(l)}$, respectively. This becomes apparent by the following commutative diagram, which summarizes the evaluation cycle:



The procedure is summarized as follows: Starting with a prescribed $\mathbf{C}_p \in W$, an approximate solution $\bar{\mathbf{q}}_{(l)} = f_{(l)}(\mathbf{C}_p)$ is obtained numerically. The configuration of limb l must then be adapted by solving the intra-limb constraints, evaluating $\bar{\boldsymbol{\vartheta}}_{(l)} = \boldsymbol{\psi}_{(l)}(\bar{\mathbf{q}}_{(l)})$. The corresponding platform pose is then obtained by evaluating $\bar{\mathbf{C}}_p = \boldsymbol{\psi}_{p(l)}(\bar{\boldsymbol{\vartheta}}_{(l)})$. The discrepancy of \mathbf{C}_p and $\bar{\mathbf{C}}_p$ is then used to update $\mathbf{q}_{(l)}$ again in the next iteration cycle.

4.1.1 Inverse Kinematics of Limb —Outer-Loop

The evaluation cycle gives rise to a nested iterative Newton-Raphson scheme. For prescribed $\mathbf{C}_p \in W$, the outer-loop computes $\mathbf{q}_{(l)} = f_{(l)}(\mathbf{C}_p)$ so that $\mathbf{C}_p = \boldsymbol{\varphi}_{p(l)}(\mathbf{q}_{(l)})$, while the inner-loop evaluates $\boldsymbol{\vartheta}_{(l)} = \boldsymbol{\psi}_{(l)}(\mathbf{q}_{(l)})$ by solving the intra-limb constraints, which is used in the outer-loop to evaluate $\boldsymbol{\varphi}_{p(l)} = \boldsymbol{\psi}_{(l)} \circ \boldsymbol{\psi}_{p(l)}(\mathbf{q}_{(l)})$.

Consider the PKM in an initial state. Let $\boldsymbol{\vartheta}_{(l),0} \in V_l$ be an admissible initial configuration of the PKM, and $\mathbf{C}_{p,0}$ be the corresponding platform pose. Given a desired platform pose $\mathbf{C}_p \in W$, the task is to compute the corresponding configuration $\boldsymbol{\vartheta}_{(l)} = \boldsymbol{\vartheta}_{(l),0} + \Delta\boldsymbol{\vartheta}_{(l)}$ starting from $\boldsymbol{\vartheta}_{(l),0}$. Firstly, this necessitates a geometrically consistent expression for the increment of the platform pose. The configuration increment, represented in the platform frame \mathcal{F}_p , is $\Delta\mathbf{C}_p = \mathbf{C}_{p,0}^{-1}\mathbf{C}_p \in SE(3)$. Its first-order approximation yields $\Delta\mathbf{C}_p \approx \mathbf{I} - \widehat{\mathbf{L}_{p(l)}\Delta\mathbf{q}_{(l)}} \in se(3)$, and thus in vector form $(\mathbf{I} - \Delta\mathbf{C}_p)^\vee = \mathbf{L}_{p(l)}\Delta\mathbf{q}_{(l)}$ ¹. The $\delta_{p(l)}$

¹ $\mathbf{A}^\vee \in \mathbb{R}^6$ is the vector corresponding to matrix $\mathbf{A} \in se(3)$. The inverse operation $\widehat{\mathbf{X}} \in se(3)$ assigns a $se(3)$ -matrix to vector $\mathbf{X} \in \mathbb{R}^6$. See appendix B.

components of this configuration increment corresponding to the platform motion are extracted with a $\delta_{p(l)} \times 6$ matrix $\mathbf{P}_{t(l)}$. Relation (25) then leads to $\mathbf{D}_{t(l)} \mathbf{P}_{t(l)} (\mathbf{I} - \Delta \mathbf{C}_p)^\vee = \mathbf{L}_{t(l)} \Delta \mathbf{q}_{(l)}$. The increment of generalized coordinates is thus approximated as

$$\Delta \mathbf{q}_{(l)} = \mathbf{F}_{t(l)} \mathbf{P}_{t(l)} (\mathbf{I} - \Delta \mathbf{C}_p)^\vee = \mathbf{F}_{t(l)} \Delta \mathbf{x}_p, \quad \text{with } \Delta \mathbf{x}_p := \mathbf{P}_{t(l)} (\mathbf{I} - \Delta \mathbf{C}_p)^\vee \quad (31)$$

and the generalized coordinates are approximated as $\mathbf{q}_{(l)} = \mathbf{q}_{(l),0} + \Delta \mathbf{q}_{(l)}$.

In case of the IRSBot-2, the platform at a separated limb has $\delta_{p(l)} = 3$ DOF, and its spatial translation is used as independent motion component. The corresponding 3×6 selection matrix is

$$\mathbf{P}_{t(l)} = \begin{pmatrix} 0 & 0 & 0 & 1 & 0 & 0 \\ 0 & 0 & 0 & 0 & 1 & 0 \\ 0 & 0 & 0 & 0 & 0 & 1 \end{pmatrix}. \quad (32)$$

Invoking (20), the increment of tree-joint variables is approximated as $\Delta \boldsymbol{\vartheta}_{(l)} = \mathbf{H}_{(l)} \Delta \mathbf{q}_{(l)}$. This step is applied iteratively until $\mathbf{C}_p = \boldsymbol{\varphi}_{p(l)}(\mathbf{q}_{(l)})$ is satisfied. Since $\mathbf{F}_{t(l)}(\boldsymbol{\vartheta}_{(l)})$ depends on the tree-joint variables, and $\boldsymbol{\varphi}_{p(l)}$ rests on a constraint solution, iterative application of this step must involve a subsequent correction of $\boldsymbol{\vartheta}_{(l)}$ in order to satisfy the intra-limb constraints. To this end, a nested iterative solution scheme is introduced as Algorithm 1.

Algorithm 1: Iterative Solution of Inverse Kinematics of Limb —Outer-Loop

Input: $\boldsymbol{\vartheta}_{(l),0}, \mathbf{C}_p$

Initialization: $\mathbf{q}_{(l)} := \mathbf{q}_{(l),0}, \boldsymbol{\vartheta}_{(l)} := \boldsymbol{\vartheta}_{(l),0}, \bar{\mathbf{C}}_p := \boldsymbol{\psi}_{p(l)}(\boldsymbol{\vartheta}_{(l),0}), \Delta \mathbf{C}_p := \bar{\mathbf{C}}_p^{-1} \mathbf{C}_p, \Delta \mathbf{x}_t := \mathbf{P}_{t(l)} (\mathbf{I} - \Delta \mathbf{C}_p)^\vee$

Outer-Loop: WHILE $\|\Delta \mathbf{x}_t\| > \varepsilon$ DO

$\Delta \mathbf{q}_{(l)} := \mathbf{F}_{t(l)} \Delta \mathbf{x}_t$

$\mathbf{q}_{(l)} := \mathbf{q}_{(l)} + \Delta \mathbf{q}_{(l)}$

$\boldsymbol{\vartheta}_{(l)} := \boldsymbol{\psi}_{(l)}(\mathbf{q}_{(l)})$ Algorithm 2 (Inner-loop, evaluated with $\boldsymbol{\vartheta}_{(l)}$)

$\bar{\mathbf{C}}_p := \boldsymbol{\psi}_{p(l)}(\boldsymbol{\vartheta}_{(l)})$ (evaluate eq. (4))

$\Delta \mathbf{C}_p := \bar{\mathbf{C}}_p^{-1} \mathbf{C}_p$

$\Delta \mathbf{x}_t := \mathbf{P}_{t(l)} (\mathbf{I} - \Delta \mathbf{C}_p)^\vee$

END

Output: $\boldsymbol{\vartheta}_{(l)}$

Notice that there is no bi-invariant metric on $SE(3)$. For computing $\|\Delta \mathbf{x}_t\|$ the left-invariant metric is used, which depends on the scaling [41, 42]. The corresponding norm of $\mathbf{X} = (\boldsymbol{\xi}, \boldsymbol{\eta})^T \in \mathbb{R}^6 \cong se(3)$ is $\|\mathbf{X}\| = \alpha \|\boldsymbol{\xi}\| + \beta \|\boldsymbol{\eta}\|$.

4.1.2 Iterative Solution of Intra-Limb Constraints —Inner-Loop

As the solution is generally not unique, this solution $\boldsymbol{\vartheta}_{(\lambda,l)} = \boldsymbol{\psi}_{(\lambda,l)}(\mathbf{q}_{(\lambda,l)})$ is valid in a neighborhood of the starting configuration. The constraints are solved with an iterative Newton-Raphson scheme. The solution of constraints (12) is evaluated numerically for given $\mathbf{q}_{(\lambda,l)}$ starting from an admissible initial configuration $\boldsymbol{\vartheta}_{(\lambda,l),0} = (\mathbf{y}_{(\lambda,l),0}, \mathbf{q}_{(\lambda,l),0}) \in V_l$. The prescribed increment of generalized coordinates is $\Delta \mathbf{q}_{(\lambda,l)} = \mathbf{q}_{(\lambda,l)} - \mathbf{q}_{(\lambda,l),0}$. The solution for the dependent coordinates is expressed as $\mathbf{y}_{(\lambda,l)} = \mathbf{y}_{(\lambda,l),0} + \Delta \mathbf{y}_{(\lambda,l)}$. A Newton-Raphson iteration scheme is constructed by linearizing the geometric constraints at the current configuration assuming sufficiently small $\Delta \mathbf{y}_{(\lambda,l)}$. First-order Taylor expansion of (12) yields $g_{(\lambda,l)}(\boldsymbol{\vartheta}_{(\lambda,l),0}) + \mathbf{G}_{\mathbf{y}_{(\lambda,l)}}(\boldsymbol{\vartheta}_{(\lambda,l),0}) \Delta \mathbf{y}_{(\lambda,l)} + \mathbf{G}_{\mathbf{q}_{(\lambda,l)}}(\boldsymbol{\vartheta}_{(\lambda,l),0}) \Delta \mathbf{q}_{(\lambda,l)} = \mathbf{0}$. In the following, the index (λ, l) is omitted for sake of simplicity, as the derivation always refers to FC λ of limb l . The solution of the overall system of linearized constraints is

$$\begin{pmatrix} \Delta \mathbf{y} \\ \Delta \mathbf{q} \end{pmatrix} = \begin{pmatrix} -\mathbf{G}_{\mathbf{y}}^{-1}(\boldsymbol{\vartheta}_0) & -\mathbf{G}_{\mathbf{y}}^{-1}(\boldsymbol{\vartheta}_0) \mathbf{G}_{\mathbf{q}}(\boldsymbol{\vartheta}_0) \\ \mathbf{0} & \mathbf{I} \end{pmatrix} \begin{pmatrix} g(\boldsymbol{\vartheta}_0) \\ \mathbf{q} - \mathbf{q}_0 \end{pmatrix}. \quad (33)$$

The so obtained coordinates $\boldsymbol{\vartheta}_0 + \Delta \boldsymbol{\vartheta}$ will not satisfy the constraints. Starting from an admissible configuration $\boldsymbol{\vartheta}_0$, i.e. $g(\boldsymbol{\vartheta}_0) = \mathbf{0}$, this gives rise to the following Newton-Raphson iteration scheme in Algorithm 2.

Algorithm 2: Iterative Solution of Loop Constraints —Inner-Loop

Input: $\vartheta_0 = (\mathbf{y}_0, \mathbf{q}_0), \Delta \mathbf{q}$

Initial Step: $\mathbf{q} := \mathbf{q}_0 + \Delta \mathbf{q}$
 $\Delta \mathbf{y} := -\mathbf{G}_y^{-1}(\vartheta_0) \mathbf{G}_q(\vartheta_0) \Delta \mathbf{q}$
 $\vartheta := (\mathbf{y}_0 + \Delta \mathbf{y}, \mathbf{q})$

Correction Steps: WHILE $\|g(\vartheta)\| > \varepsilon$ DO
 $\Delta \mathbf{y} := -\mathbf{G}_y^{-1}(\vartheta) \mathbf{g}(\vartheta)$
 $\vartheta := (\mathbf{y} + \Delta \mathbf{y}, \mathbf{q})$
END

Output: $\vartheta = (\mathbf{y}, \mathbf{q})$

This evaluates the solution $\vartheta_{(\lambda,l)} = \Psi_{(\lambda,l)}(\mathbf{q}_{(\lambda,l)})$ of loop constraints of FC $\Lambda_{(\lambda,l)}$, and thus the overall solution (15) in terms of the δ_l generalized coordinates $\mathbf{q}_{(l)}$, as they are independent for a hybrid limb. The iteration scheme is a computationally efficient and numerically stable solution method, which converges after a few iteration steps, provided that $\mathbf{G}_y(\lambda,l)$ or $\mathbf{G}_q(\lambda,l)$ are well conditioned (which is not the case near singularities).

Remark 6. A solution can also be obtained by numerical time integration of the velocity constraints. This is pursued for numerical time integration of the EOM of general MBS, e.g. in index 2 formulation. Then, constraint violations due to numerical drift must be stabilized, however [57, 58, 59]. A simple method is the Baumgarte stabilization, which ensures asymptotic decay of the error over time. When the model is used to compute the feedforward command in model-based control schemes, an asymptotic decay is not sufficient.

4.2 Simplified iteration scheme —Compound iteration step for inverse kinematics and loop constraints

The nested solution scheme separates the solution of loop constraints from that of the inverse kinematics of the limbs. Algorithm 2 performs exactly as many steps as necessary for the individual constraints. This allows dealing with ill-conditioned or redundant loop constraints for particular loops, while not increasing the number of iterations for solving the limb inverse kinematics. On the other hand, if all subproblems are well-conditioned, the loop constraints and inverse kinematics can be solved using a one overall iteration step. In other words, one single step in algorithm 2, for solving loop constraints, is performed per step of algorithm 1. This is summarized as Algorithm 3.

Algorithm 3: Compound Scheme solving Inverse Kinematics of Limb along with Loop Constraints

Input: $\vartheta_{(l),0}, \mathbf{C}_p$

Initialization: $\vartheta_{(l)} := \vartheta_{(l),0}, \bar{\mathbf{C}}_p := \Psi_{p(l)}(\vartheta_{(l),0}), \Delta \mathbf{C}_p := \bar{\mathbf{C}}_p^{-1} \mathbf{C}_p, \Delta \mathbf{x}_t := \mathbf{P}_{t(l)} (\mathbf{I} - \Delta \mathbf{C}_p)^\vee$

Outer-Loop: WHILE $\|\Delta \mathbf{x}_t\| > \varepsilon_1 \vee \|g(\vartheta_{(l)})\| > \varepsilon_2$ DO
 $\Delta \vartheta_{(l)} := \mathbf{H}_{(l)}(\vartheta_{(l)}) \mathbf{F}_{t(l)}(\vartheta_{(l)}) \mathbf{P}_t (\mathbf{I} - \Delta \mathbf{C}_p)^\vee$
 $\vartheta_{(l)} := \vartheta_{(l)} + \Delta \vartheta_{(l)}$
 $\bar{\mathbf{C}}_p := \Psi_{p(l)}(\vartheta_{(l)})$ (evaluate eq. (4))
 $\Delta \mathbf{C}_p := \bar{\mathbf{C}}_p^{-1} \mathbf{C}_p$
 $\Delta \mathbf{x}_t := \mathbf{P}_{t(l)} (\mathbf{I} - \Delta \mathbf{C}_p)^\vee$
END

Output: $\vartheta_{(l)}$

4.3 Comparison with standard MBS formulations

Many of the proposed lower-mobility PKM with complex limbs [26,62,63] are (globally) overconstrained, which is reflected by a redundant overall system of constraints. This is problematic when using standard MBS modeling approaches. The local constraint embedding alleviates this problem as for many (globally) overconstrained PKM, the intra-limb constraints are not redundant. This is briefly discussed next.

Relative coordinate formulation In the relative coordinate formulation, a spanning tree is introduced for the PKM as a whole. For example, a possible tree on the topological graph Γ in fig. 2a) is shown in fig. 3. Three U joints and two R joints are removed, which leaves a tree-topology MBS with $n = 5 \cdot 2 + 3 \cdot 1 = 13$ tree-joint variables (5 U- & 3 R-joints). A system of $m_{\text{rel}} = 3 \cdot 4 + 2 \cdot 5 = 22$ cut-joint constraints (3 U- & 2 R-joints) is introduced. Clearly, 7 of the 22 constraints are redundant as the PKM DOF is $\delta = 2$. If the information that the R-joints form planar mechanisms, and only 2 constraints are imposed per loop, then there are 16 cut-joint constraints and still 5 of them are redundant.

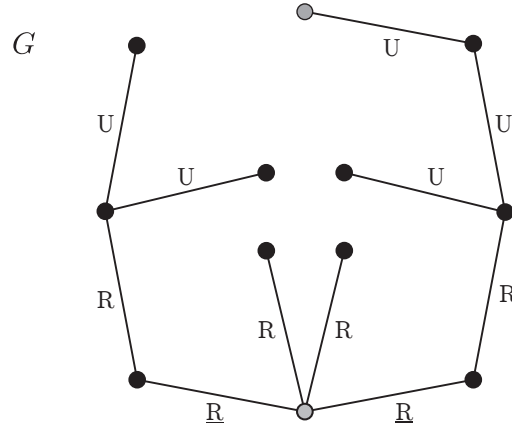


Fig. 3. A possible tree G on the topological graph Γ of the IRSBot-2 in fig. 2a).

Absolute coordinate formulation The absolute coordinate formulation is another established approach in computational MBS dynamics [8]. It leads to a large but sparse system of EOM where the constraint Jacobian is sparse reflecting the local topological loops and the overall PKM topology. The rank deficiency is the same as in the relative coordinate formulation. The absolute coordinate model explicitly involves the constraint reactions (Lagrange multipliers). This information is useful for trajectory planning and can be used for limiting the joint loads [64], while for control purposes, the minimal coordinate model is preferable.

Local constraint embedding The L inter-limb constraints give rise to the overall system of $m = m_1 + \dots + m_l$ constraints. As with the relative coordinate model, these constraints are redundant for overconstrained (lower-mobility) PKM. Instead of imposing a system of m constraints, the local constraint embedding technique imposes the particular intra-limb constraints to the separated kinematic loops, and incorporates their solutions into the model. It thus avoids dealing with a singular overall constraints system. Even if the intra-limb constraints are redundant, reflected by singular Jacobians $\mathbf{G}_{(\lambda,l)}$ in (13), the local constraint embedding method allows dealing with this locally. Moreover, many lower-mobility PKM are globally overconstrained but the separated limbs are not overconstrained. The IRSBot-2, for instance, is overconstrained leading to a redundant overall system of $m_{\text{rel}} = 22$ constraints (see above). On the other hand, the intra-limb constraints for the 4U loop is regular, and those for the planar 4R loop can be non-redundantly formulated (see section 6). That is, the overconstrained problem is avoided by the local constraint embedding. Moreover, the embedding technique renders the PKM model as a model of PKM with simple limbs. This allows for modeling in terms of task space coordinates, by combining the models of the L limbs, and thus treating complex [24] and simple limbs [60] in a unified way.

5 Dynamics Equations of Motion

A task space formulation of the dynamic EOM of PKM with complex limbs was derived in [24], and for PKM with simple limbs in [27, 26, 60] by combining the EOM of the L limbs using the inverse kinematics solution (27) in terms of the generalized coordinates $\mathbf{q}_{(l)}$. In the following, the inverse kinematics solution computed with the constraint embedding technique is used. In this formulation, the platform is treated separately, and the EOM of limb l in terms of $\mathbf{q}_{(l)}$ are constructed from the EOM of the tree-topology system using the solution (20) of the intra-limb constraints. For the IRSBot-2 example, Fig. 4 shows the kinematic topology of the system for which the EOM are constructed that are then combined to the overall EOM, which comprises two tree-systems for the limbs and the single platform body.

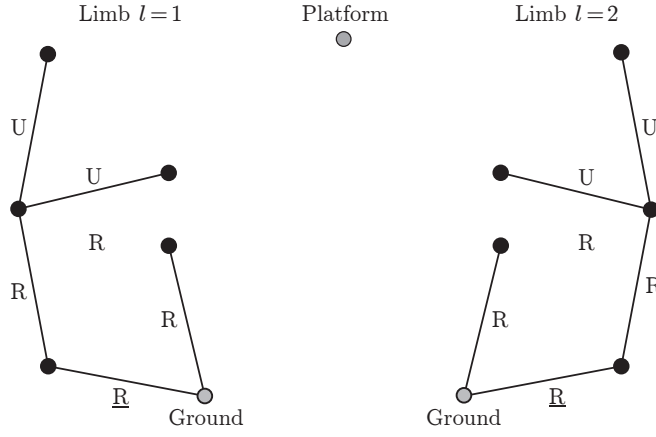


Fig. 4. Kinematic topology of the system for which EOM are derived in case of the IRSBot-2.

5.1 EOM of Tree-Topology System of a Limb

The platform and the joint connecting it to limb l are removed from the tree-topology system associated to the limb. Denote with $\bar{\vartheta}_{(l)} \in \mathbb{V}^{\bar{n}_l}$ the vector of the remaining \bar{n}_l tree-joint coordinates. The EOM of this system can be written in the standard form for tree-topology MBS

$$\bar{\mathbf{M}}_{(l)} \ddot{\bar{\vartheta}}_{(l)} + \bar{\mathbf{C}}_{(l)} \dot{\bar{\vartheta}}_{(l)} + \bar{\mathbf{Q}}_{(l)}^{\text{grav}} + \bar{\mathbf{Q}}_{(l)} = \bar{\mathbf{Q}}_{(l)}^{\text{act}} \quad (34)$$

Therein, $\bar{\mathbf{M}}_{(l)}(\bar{\vartheta}_{(l)})$ is the generalized mass matrix, $\bar{\mathbf{C}}_{(l)}(\dot{\bar{\vartheta}}_{(l)}, \bar{\vartheta}_{(l)})$ is the Coriolis/centrifugal matrix, $\bar{\mathbf{Q}}_{(l)}^{\text{grav}}(\bar{\vartheta}_{(l)})$ represents generalized gravity forces, and $\bar{\mathbf{Q}}_{(l)}$ accounts for all remaining forces (e.g. friction). The vector $\bar{\mathbf{Q}}_{(l)}^{\text{act}}(t)$ accounts for actuation forces. Its non-zero entries are the torques/forces at the actuated joints. The EOM (34) can be expressed in a compact and readily implemented form employing the system matrices $\mathbf{J}_{(l)}, \mathbf{A}_{(l)}, \mathbf{a}_{(l)}$ used for the kinematics modeling in sec. 3. Details can be found in [24, 40, 47].

5.2 EOM of Complex Limb without Platform

The joint velocity of the tree-system is determined with (20) by the generalized velocities. The joint velocities of the system without platform can thus be written as

$$\dot{\bar{\vartheta}}_{(l)} = \bar{\mathbf{H}}_{(l)} \dot{\bar{\mathbf{q}}}_{(l)}. \quad (35)$$

where $\bar{\mathbf{H}}_{(l)}(\vartheta_{(l)})$ is the $\bar{n}_l \times \delta_l$ submatrix of $\mathbf{H}_{(l)}$ with rows corresponding to the \bar{n}_l tree-joint variables. Using variations $\delta \dot{\bar{\vartheta}}_{(l)} = \bar{\mathbf{H}}_{(l)} \delta \dot{\bar{\mathbf{q}}}_{(l)}$, along with (35) and its derivative, the principle of virtual power yields the EOM of the complex limb

$$\bar{\bar{\mathbf{M}}}_{(l)} \ddot{\bar{\mathbf{q}}}_{(l)} + \bar{\bar{\mathbf{C}}}_{(l)} \dot{\bar{\mathbf{q}}}_{(l)} + \bar{\bar{\mathbf{Q}}}_{(l)}^{\text{grav}} + \bar{\bar{\mathbf{Q}}}_{(l)} = \bar{\bar{\mathbf{Q}}}_{(l)}^{\text{act}} \quad (36)$$

where

$$\begin{aligned} \bar{\bar{\mathbf{M}}}_{(l)}(\vartheta_{(l)}) &:= \bar{\mathbf{H}}_{(l)}^T \bar{\mathbf{M}}_{(l)} \bar{\mathbf{H}}_{(l)} \\ \bar{\bar{\mathbf{C}}}_{(l)}(\vartheta_{(l)}, \dot{\vartheta}_{(l)}) &:= \bar{\mathbf{H}}_{(l)}^T (\bar{\mathbf{M}}_{(l)} \dot{\bar{\mathbf{H}}}_{(l)} + \bar{\mathbf{C}}_{(l)} \bar{\mathbf{H}}_{(l)}) \\ \bar{\bar{\mathbf{Q}}}_{(l)}(\vartheta_{(l)}) &:= \bar{\mathbf{H}}_{(l)}^T \bar{\mathbf{Q}}_{(l)}, \quad \bar{\bar{\mathbf{Q}}}_{(l)}^{\text{act}}(\vartheta_{(l)}) := \bar{\mathbf{H}}_{(l)}^T \bar{\mathbf{Q}}_{(l)}^{\text{act}} \\ \bar{\bar{\mathbf{Q}}}_{(l)}^{\text{grav}}(\vartheta) &:= \bar{\mathbf{H}}_{(l)}^T \bar{\mathbf{Q}}_{(l)}^{\text{grav}}. \end{aligned} \quad (37)$$

The EOM (36) constitute a system of δ_l ODEs in terms of the generalized velocities $\dot{\bar{\mathbf{q}}}_{(l)}$ and acceleration $\ddot{\bar{\mathbf{q}}}_{(l)}$. Since the geometric loop constraints cannot be solved explicitly, all terms remain dependent on the tree-joint variables $\vartheta_{(l)}$ (the joint

variables of the complete tree-system, including the joints connecting the platform with the limbs). The latter are determined in terms of the generalized coordinates with the numerical solution of the form $\vartheta_{(l)} = \Psi_{(l)}(\mathbf{q}_{(l)})$, computed with the solution scheme of section 4.1.2.

5.3 Task Space Formulation of PKM Dynamics

The platform dynamics is not governed by the above EOM. The dynamics of the platform as a floating rigid body is governed by the Newton-Euler equations, which are expressed as

$$\mathbf{M}_p \dot{\mathbf{V}}_p + \mathbf{G}_p \mathbf{M}_p \mathbf{V}_p + \mathbf{W}_p^{\text{grav}} = \mathbf{W}_p^{\text{EE}}. \quad (38)$$

Here \mathbf{M}_p is the constant mass matrix expressed in the platform frame \mathcal{F}_p , and matrix $\mathbf{G}_p(\mathbf{V}_p) = -\mathbf{ad}_{\mathbf{V}_p}^T$ accounts for gyroscopic and centrifugal effects [24]. The wrenches $\mathbf{W}_p^{\text{grav}}$ and \mathbf{W}_p account for gravity and the interaction of the PKM via the EE.

With the EOM of all components in place, the overall EOM in terms of the task space velocity are obtained with the inverse kinematics solution (27). Accordingly, the principle of virtual power with variations $\delta \dot{\mathbf{q}}_{(l)} = \bar{\mathbf{F}}_{(l)} \delta \mathbf{V}_t$ yields the EOM

$$\mathbf{M}_t \dot{\mathbf{V}}_t + \mathbf{C}_t \mathbf{V}_t + \mathbf{W}_t^{\text{grav}} + \mathbf{W}_t = \mathbf{W}_t^{\text{EE}} + \mathbf{J}_{\text{IK}}^T \mathbf{u}(t) \quad (39)$$

with the $\delta \times \delta$ generalized mass matrix and Coriolis matrix

$$\mathbf{M}_t(\vartheta) := \sum_{l=1}^L \bar{\mathbf{F}}_{(l)}^T \bar{\mathbf{M}}_{(l)} \bar{\mathbf{F}}_{(l)} + \mathbf{P}_p^T \mathbf{M}_p \mathbf{P}_p \quad (40)$$

$$\mathbf{C}_t(\vartheta, \dot{\vartheta}) := \sum_{l=1}^L \bar{\mathbf{F}}_{(l)}^T (\bar{\mathbf{C}}_{(l)} \bar{\mathbf{F}}_{(l)} + \bar{\mathbf{M}}_{(l)} \dot{\bar{\mathbf{F}}}_{(l)}) + \mathbf{P}_p^T \mathbf{G}_p \mathbf{M}_p \mathbf{P}_p \quad (41)$$

where the gyroscopic matrix in (38) is evaluated with the task space velocity, using (11), as $\mathbf{G}_p = \mathbf{G}_p(\mathbf{P}_p \mathbf{V}_t)$. The generalized forces accounting for EE-loads, gravity, and all remaining forces are

$$\mathbf{W}_t^{\text{EE}}(t) := \mathbf{P}_p^T \mathbf{W}_p^{\text{EE}}(t) \quad (42)$$

$$\mathbf{W}_t^{\text{grav}}(\vartheta, \mathbf{x}) := \sum_{l=1}^L \bar{\mathbf{F}}_{(l)}^T \bar{\mathbf{Q}}_{(l)}^{\text{grav}} + \mathbf{P}_p^T \mathbf{W}_p^{\text{grav}} \quad (43)$$

$$\mathbf{W}_t(\vartheta, \dot{\vartheta}, t) := \sum_{l=1}^L \bar{\mathbf{F}}_{(l)}^T \bar{\mathbf{Q}}_{(l)}. \quad (44)$$

The vector $\mathbf{u} \in \mathbb{R}^{N_{\text{act}}}$ of $N_{\text{act}} \geq \delta$ actuator forces/torques yields the corresponding generalized forces via the inverse kinematics Jacobian $\mathbf{J}_{\text{IK}}(\vartheta)$ in (30). All terms in (39) dependent on the tree-joint variables ϑ of all limbs (including joint connecting limbs and platform).

5.4 Implementation and Application Aspects

The task space formulation is particularly advantageous for model-based control where the solution to the inverse dynamics problem delivers the feed-forward control command

$$\mathbf{u} = \mathbf{J}_{\text{IK}}^{-T} (\mathbf{M}_t \dot{\mathbf{V}}_t + \mathbf{C}_t \mathbf{V}_t + \mathbf{W}_t^{\text{grav}} + \mathbf{W}_t - \mathbf{W}_t^{\text{EE}}). \quad (45)$$

In this regard, its computational efficiency is crucial. The formulation efficiently separates the kinematics modeling of limbs and PKM from the dynamics modeling. Consequently, the formalism to evaluate the EOM (34) of the limbs can be chosen as appropriate or according to computational preferences. This could be a classical MBS relative coordinate formalism [1, 2, 3] or a Lie group method [24, 40, 47]. The latter offer a user-friendly modeling approach while ensuring

computational efficiency. A Lie group formulation employing the notation used in this paper can be found in [24, appendix B].

Depending on the complexity of the PKM, the computational efficiency can further be improved by recursively evaluating the EOM (34) of the limbs using $O(n)$ algorithms [65, 66], instead of deriving them in closed form. Moreover, the topological independence of the limbs allows for evaluating the EOM (36) in parallel. Invoking the constraint embedding method, an $O(n)$ algorithm was proposed in [28, 9, 30] where for each FC $\Lambda_{\lambda(l)}$ an aggregated mass matrix is introduced, which is obtained by introducing the solution of the constraints. Then, for a hybrid limb, the limb reduces to a serial chain of aggregated bodies (each representing a FC) whose dynamics can be evaluated in $O(n)$.

The topology of PKM naturally allows for a modular modeling approach. Moreover, since (34) are the EOM of a separated limb without the platform, and since the majority of PKM consists of structurally identical limbs, the EOM (34) and (36) can be derived (or evaluated) for a prototypical limb, and incorporated into the overall EOM (39). This has been described in detail in [60, 24].

Another benefit of formulating the EOM in task space in general is that the terms in the EOM reveal the dynamic properties of the PKM as apparent in task space. In particular the mass matrix \mathbf{M}_t characterizes the apparent inertia at the EE. This is also called the reflected mass, which is an information used to assess a PKM when used as collaborative robot and in human machine interaction (HMI) scenarios [67].

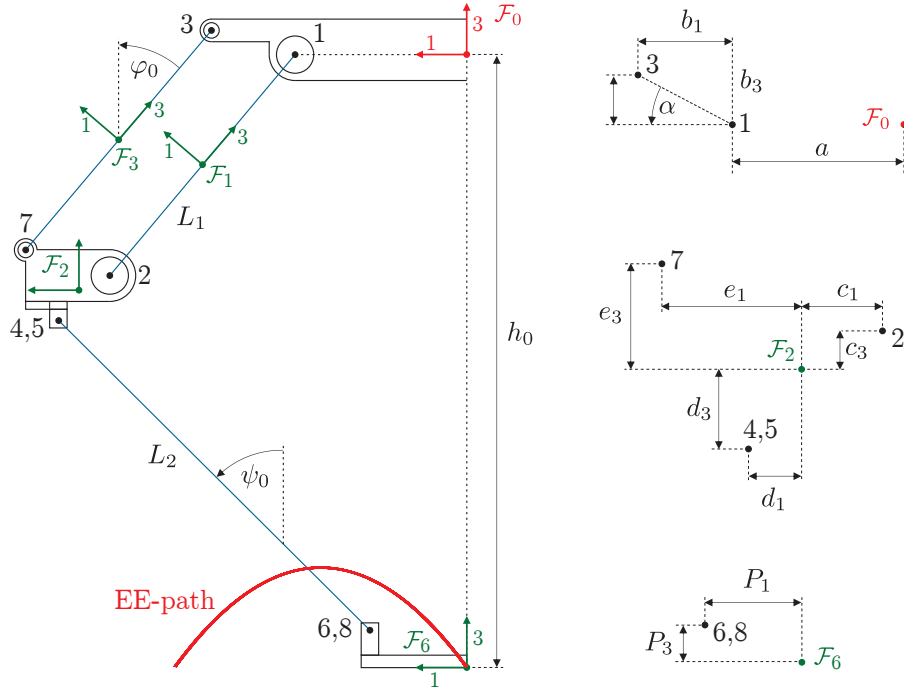
5.5 Constraint Embedding, Aggregated bodies, and $O(n)$ Formulations

Since the constraint embedding method casts the complex limbs of a PKM as serial kinematic chain obtained by aggregating all bodies of a FC. The FC are represented by a submechanism with its own internal dynamics, described by a set of independent generalized coordinates. Each of this submechanisms is referred to as an aggregated body [9]. That is, the hybrid limb can be regarded as an aggregated tree where each aggregated body, i.e. each loop of the hybrid limb, is represented by a (configuration dependent) mass matrix. The latter are $\mathbf{H}_{(\lambda,l)}^T \mathbf{M}_{(\lambda,l)} \mathbf{H}_{(\lambda,l)}$, where $\mathbf{M}_{(\lambda,l)}$ is the submatrix of $\bar{\mathbf{M}}_{(l)}$ associated to the FC $\Lambda_{\lambda(l)}$.

6 Example: IRSBot-2

In the following, numerical results are presented for the IRSBot-2 when the inverse kinematics is solved with the constraint embedding method, and the inverse dynamics is solved subsequently. The dynamic parameters are simplified for simplicity, and since no particular data is available.

Fig. 5. Geometry of the IRSBot-Model – Front view of right limb. φ_0 and ψ_0 describe the orientation of the proximal and distal limb, and h_0 is the platform height in the reference configuration $\vartheta = \mathbf{0}$, respectively.



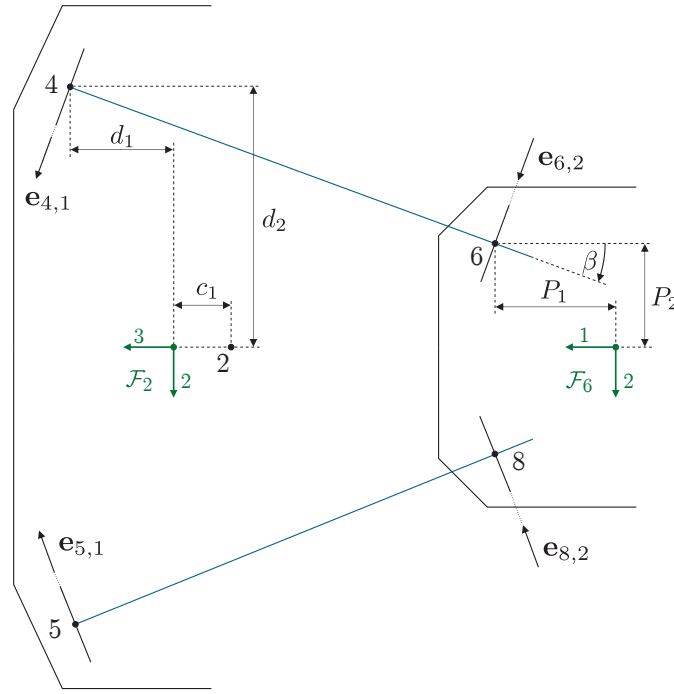


Fig. 6. Geometry of the distal limb of the IRSBot-Model – Top view of the right limb. $\mathbf{e}_{4,1}$ and $\mathbf{e}_{5,1}$ are unit vectors along the first revolute axis of U-joint 4 and 5, and $\mathbf{e}_{6,2}$ and $\mathbf{e}_{8,2}$ are unit vectors along the second revolute axis of U-joint 6 and 8 respectively.

6.1 Kinematics of tree-topology system

Joint variables: The tree-topology system for limb $l = 1, 2$ is introduced according to the spanning tree $\vec{G}_{(l)}$ in Fig. 2c). It consists of the three R-joints 1,2,3, and the three U-joints 4,5,6. The revolute joint angles are denoted with $\varphi_{1(l)}, \varphi_{2(l)}, \varphi_{3(l)}$. The U-joints are modeled as combination of two R-joints with revolute angles $\varphi_{4,1(l)}, \varphi_{4,2(l)}, \varphi_{5,1(l)}, \varphi_{5,2(l)}, \varphi_{6,1(l)}, \varphi_{6,2(l)}$. The nine revolute angles form the joint coordinate vector $\vartheta_{(l)} \in \mathbb{V}^9$. All joint angles are measured according to the spanning tree.

Geometric parameters: The limb geometry is parameterized as shown in Fig. 5 and 6. The parameters satisfy the following relations

$$\begin{aligned}
 b_1 &= b \cos \alpha, \quad b_3 = b \sin \alpha, \quad e_1 = b_1 - c_1, \quad e_3 = b_3 + c_3 \\
 \sin \beta &= \frac{d_2 - p_2}{\sqrt{u^2 + (d_2 - p_2)^2}} = \frac{1}{\sqrt{u^2 + 1/\tan^2 \beta}}, \quad \cos \beta = \frac{u}{\sqrt{u^2 + (d_2 - p_2)^2}} = \frac{1}{\sqrt{1 + \tan^2 \beta}}, \quad \tan \beta = \frac{d_2 - p_2}{u} \quad (46) \\
 \sin \psi_0 &= \frac{\sqrt{(d_2 - p_2)^2 + u^2}}{L_2}, \quad \cos \psi_0 = \frac{\sqrt{L_2^2 - (d_2 - p_2)^2 - u^2}}{L_2}, \quad \text{with } u := a + c_1 + d_1 - p_1 + L_1 \sin \varphi_0.
 \end{aligned}$$

For numerical computations, the following parameter values are selected so to approximately resemble the IRSBot-2 design

$$\begin{aligned}
 a &= 1/8 \text{ m}, \quad b = 1/12 \text{ m}, \quad c_1 = b_1/2, \quad c_3 = b_3, \quad d_1 = b_1/2, \quad d_2 = a, \quad d_3 = c_3, \\
 L_1 &= 1/4 \text{ m}, \quad L_2 = 1/2 \text{ m}, \quad P_1 = a/2, \quad P_2 = d_2/2, \quad P_3 = 0, \quad \alpha = \pi/6, \quad \varphi_0 = \pi/4. \quad (47)
 \end{aligned}$$

Joint screw coordinates: Basis for the kinematics modeling, are the joint screw coordinates in (2), which are defined as

$$\mathbf{Y}_{i(l)} = (\mathbf{e}_{i(l)}, \mathbf{y}_{i(l)} \times \mathbf{e}_{i(l)})^T, \quad l = 1, 2 \quad (48)$$

where $\mathbf{y}_{i(l)} \in \mathbb{R}^3$ denotes the position vector of a point on the axis of joint i , and $\mathbf{e}_{i(l)} \in \mathbb{R}^3$ is a unit vector along the axis. Both vectors are resolved in the spatial IFR \mathcal{F}_0 shown in Fig. 1b). In the zero reference configuration in Fig. 1, the joint

position and unit direction vectors are thus

$$\begin{aligned}
\mathbf{y}_1 &= (a, 0, 0)^T, \mathbf{y}_2 = (a + L_1 \sin \varphi_0, 0, -L_1 \cos \varphi_0)^T, \mathbf{y}_3 = (a + b_1, 0, b_3)^T \\
\mathbf{y}_{4,1} &= \mathbf{y}_{4,2} = (a + c_1 + d_1 + L_1 \sin \varphi_0, d_2, -c_3 - d_3 - L_1 \cos \varphi_0)^T \\
\mathbf{y}_{5,1} &= \mathbf{y}_{5,2} = (a + c_1 + d_1 + L_1 \sin \varphi_0, -d_2, -c_3 - d_3 - L_1 \cos \varphi_0)^T \\
\mathbf{y}_{6,1} &= \mathbf{y}_{6,2} = (p_1, -p_2, -c_3 - d_3 - L_1 \cos \varphi_0 - L_2 \cos \psi_0)^T \\
\mathbf{e}_1 &= \mathbf{e}_2 = \mathbf{e}_3 = (0, 1, 0), \mathbf{e}_{4,2} = \mathbf{e}_{6,1} = (\cos \beta \cos \psi_0, -\sin \beta \cos \psi_0, \sin \psi_0), \mathbf{e}_{4,1} = \mathbf{e}_{6,2} = (\sin \beta, \cos \beta, 0) \\
\mathbf{e}_{5,1} &= (-\sin(\beta), \cos(\beta), 0), \mathbf{e}_{5,2} = (\cos \beta \cos \psi_0, \sin \beta \cos \psi_0, \sin \psi_0).
\end{aligned}$$

Therein, and in the following, indexes $i, 1$ and $i, 2$ refer to the two revolute axes of U-joint i .

Reference configurations: The reference configuration $\mathbf{A}_{i(l)}$ of body $i(l)$ in (1) involves the rotation matrix $\mathbf{R}_{i(l),0} \in SO(3)$ and position vector $\mathbf{r}_{i(l),0} \in \mathbb{R}^3$ of the body-fixed frame relative to the IFR \mathcal{F}_0 . According to Figs. 5 and 6, these are

$$\begin{aligned}
\mathbf{R}_{1(l),0} &= \mathbf{R}_{3(l),0} = \text{Rot}(y, -\varphi_0), \mathbf{R}_{2(l),0} = \mathbf{R}_{6(l),0} = \mathbf{I}, \mathbf{R}_{4(l),0} = \text{Rot}(z, -\beta) \text{Rot}(y, \psi_0), \mathbf{R}_{5(l),0} = \text{Rot}(z, \beta) \text{Rot}(y, \psi_0) \\
\mathbf{r}_{1(l),0} &= (a + L_1/2 \sin \varphi_0, 0, -L_1/2 \cos \varphi_0)^T, \mathbf{r}_{2(l),0} = (a + b_1 + L_1/2 \sin \varphi_0, 0, b_3 - L_1/2 \cos \varphi_0)^T \\
\mathbf{r}_{3(l),0} &= (a + c_1 + L_1 \sin \varphi_0, 0, b_3 - L_1/2 \cos \varphi_0)^T, \mathbf{r}_{6(l),0} = (0, 0, -c_3 - d_1 - P_3 - L_1 \cos \varphi_0 - L_2 \cos \psi_0)^T \\
\mathbf{r}_{4(l),0} &= ((a + c_1 + d_1 + p_1 + L_1 \sin \varphi_0)/2, -(p_2 + d_2)/2, -c_3 - d_3 - L_1 \cos \varphi_0 - L_2/2 \cos \psi_0)^T \\
\mathbf{r}_{5(l),0} &= ((a + c_1 + d_1 + p_1 + L_1 \sin \varphi_0)/2, (p_2 + d_2)/2, -c_3 - d_3 - L_1 \cos \varphi_0 - L_2/2 \cos \psi_0)^T
\end{aligned}$$

where $\text{Rot}(y, \varphi)$ and $\text{Rot}(z, \varphi)$ denote the rotation matrices for rotations about the y - and z -axis, respectively.

6.2 Loop constraints

A single limb has two independent FC, referred to as the proximal (close to the base) and the distal loop. According to the spanning tree $\vec{G}_{(l)}$ in fig. 2c) the tree-topology system is obtained by removing revolute joint 7 and universal joint 8, for which cut-joint constraints are introduced.

Proximal loop: The proximal loop, which corresponds to FC $\Lambda_{1,l}$, is a planar parallelogram 4-bar linkage formed by the R-joints 1,2,3,7. According the spanning tree in Fig. 2c), joints 1,2,3 are tree-joints, and the vector of tree-joint coordinates consists of the $n_{1,l}$ joint angles $\vartheta_{(1,l)} = (\varphi_{1(l)}, \varphi_{2(l)}, \varphi_{3(l)})^T$. The cut-joint constraints for the revolute joint 7 thus yields $m_{1,l} = 2$ independent (translation) constraints, so that FC $\Lambda_{1,l}$ has $\delta_{1,l} = 1$ DOF. The revolute joint angle $\varphi_{1(l)}$ of the actuated joint 1 is used as independent coordinate, so that $\mathbf{q}_{(1,l)} = (\varphi_{1(l)})$ and $\mathbf{y}_{(1,l)} = (\varphi_{2(l)}, \varphi_{3(l)})^T$. The planar parallelogram 4-bar is treated ad hoc as the solution is readily known. The solution of the geometric loop constraints for FC $\Lambda_{1,l}$ is readily found as $\varphi_{1(l)} = \varphi_{3(l)} = -\varphi_{2(l)}$, and the velocity constraints are solved with

$$\mathbf{H}_{(1,l)} = \begin{pmatrix} 1 \\ -1 \\ 1 \end{pmatrix}. \quad (49)$$

Distal loop: The distal loop is formed by U-joints 4,5,6,8. The loop constraints for FC $\Lambda_{2,l}$ thus involves the $n_{2,l} = 3 \cdot 2$ tree-joint coordinates $\vartheta_{(2,l)} = (\varphi_{4,1(l)}, \varphi_{4,2(l)}, \varphi_{5,1(l)}, \varphi_{5,2(l)}, \varphi_{6,1(l)}, \varphi_{6,2(l)})^T$. The universal joint 8 imposes $m_{2,l} = 4$ cut-joint constraints. These constraints are non-redundant, and the FC $\Lambda_{2,l}$ has $\delta_{2,l} = 2$ DOF. The angles of universal joint 6 are used as independent coordinates, i.e. $\mathbf{q}_{(2,l)} = (\varphi_{6,1(l)}, \varphi_{6,2(l)})^T$, $\mathbf{y}_{(2,l)} = (\varphi_{4,1(l)}, \varphi_{4,2(l)}, \varphi_{5,1(l)}, \varphi_{5,2(l)})^T$. Constraints are introduced with the general formulation in appendix A.

The U-joint imposes three position constraints between body $k = 6 = P$ (the platform) and $r = 5$ of the form (51). In the following, the index (l) is omitted. The body-fixed position vectors, expressed in frame $\mathcal{F}_{r=5}$ and platform frame $\mathcal{F}_{k=6}$ (see Fig. 7), in (50) are ${}^k \mathbf{d}_{k,\lambda} = {}^6 \mathbf{d}_{6,2} = (P_1, P_2, P_3)^T$, ${}^r \mathbf{d}_{r,\lambda} = {}^5 \mathbf{d}_{5,2} = (0, 0, -L_2/2)^T$, with the parameters introduced above. The relative displacement vector expressed in platform frame $\mathcal{F}_{k=P}$ is ${}^k \mathbf{d}_\lambda = \mathbf{R}_{k,r}(\mathbf{r}_r - \mathbf{r}_k) + \mathbf{R}_{k,r} {}^r \mathbf{d}_{r,\lambda} - {}^k \mathbf{d}_{k,\lambda}$, where $\mathbf{R}_{k,r} = \mathbf{R}_k^T \mathbf{R}_r$, with the absolute rotation matrices $\mathbf{R}_k, \mathbf{R}_r$ of body $r = 5$ and platform $r = 6$, and their position vectors $\mathbf{r}_r, \mathbf{r}_k$, respectively, determined by (1). As no relative translation is permitted, the three position constraints are ${}^k \mathbf{d}_{k,\lambda} = \mathbf{0}$. The constraint Jacobian in (55) comprises the submatrices $\mathbf{J}_{5,2} = (\mathbf{0}, \mathbf{0}, \mathbf{J}_{5,1}, \mathbf{J}_{5,2}, \mathbf{0}, \mathbf{0})$ and $\mathbf{J}_{6,2} = (\mathbf{J}_{4,1}, \mathbf{J}_{4,2}, \mathbf{0}, \mathbf{0}, \mathbf{J}_{6,1}, \mathbf{J}_{6,2})$.

The orientation constraints (58) are formulated with ${}^r\mathbf{u}_\alpha = {}^5\mathbf{u}_\alpha = (1, 0, 0)^T$, which is the unit vector along the rotation axis of the U-joint 8 that is constant relative to body $r = 5$, and ${}^k\mathbf{u}_\beta = {}^6\mathbf{u}_\beta = (-\sin\beta, \cos\beta, 0)^T$ is the unit vector along the other rotation axis of the U-joint that is constant relative to the platform $k = 6$. The single orientation constraint is $g_{\alpha,\beta}^{\text{rot}} := {}^k\mathbf{u}_\alpha^T \mathbf{R}_{k,r} {}^r\mathbf{u}_\beta$. This, along with the three position constraints, gives rise to $m_{2,l} = 4$ loop constraints for $\Lambda_{2(l)}$. The corresponding velocity and acceleration constraints are found with (59) and (60).

Overall, the kinematics of limb l is described by $n_l = 9$ joint variables subjected to $m_l = 6$ constraints, and has $\delta_l = 3$ DOF. The solution of velocity constraints is given by (20) in terms of the independent velocities $\dot{\mathbf{q}}_{(l)} = (\dot{\phi}_{1(l)}, \dot{\phi}_{6,1(l)}, \dot{\phi}_{6,2(l)})^T$.

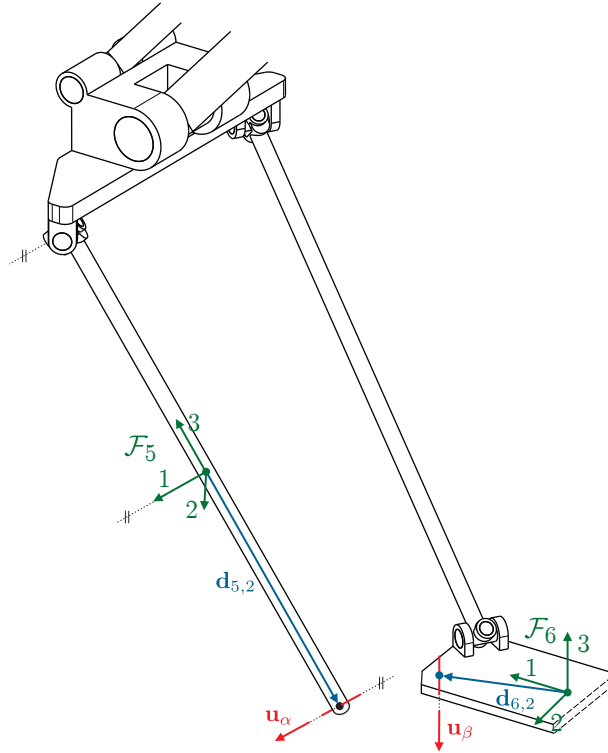


Fig. 7. Geometry of cut-joint (U-joint 8).

6.3 Inverse Kinematics

The platform attached to a separated limb of the IRSBot-2 has $\delta_l = 3$ DOF, and the spatial position of the platform can be used as independent components of the platform motion. The task space Jacobian $\mathbf{L}_{t(l)}$ in (25) thus comprises the last three rows of $\mathbf{L}_{p(l)}$. Since the platform DOF is $\delta_p = 2$, and the task velocity vector $\mathbf{V}_t = (v_1, v_3)^T$ contains two translation components only, the limbs (and thus the PKM) are non-equimobile. The generalized velocity of the separated limb $l = 1, 2$ is computed from the prescribed task velocity via (27), and the tree-joint velocities via (28), with the velocity distribution matrix $\mathbf{D}_{t(l)}$ in (26). The 2×2 inverse kinematics Jacobian \mathbf{J}_{IK} in (30) consists of the first column of $\mathbf{F}_{(1)}$ and of $\mathbf{F}_{(2)}$.

6.4 Numerical Results

The inverse dynamics is solved with a sampling time of $\Delta t = 0.01$ s. The EOM (39) were implemented in closed form, and numerically evaluated for a prescribed EE-motion using Matlab. All results were validated against the commercial MBS simulation tool Alaska [68]. With the chosen parameters, the reference position of the platform for the zero reference configuration $\vartheta = \mathbf{0}$ is $\mathbf{r}_{6,0} = (0, 0, -1/24(4 + 6\sqrt{2} + \sqrt{6(37 - 6\sqrt{2} - 2\sqrt{3} - 4\sqrt{6})}))^T$. The platform translation was prescribed as a parabolic curve $\mathbf{r}_6(t) = \mathbf{r}_{6,0} + (\Delta x \cdot s(t), 0, \Delta z \cdot 4s(t)(1 - s(t)))^T$, with motion profile $s(t) = \sin^2(\sqrt{\pi}t/T)$, and $\Delta x = 0.25$ m, $\Delta z = 0.45$ m, where the EE has to perform $v = 3$ cycles per second. The EE-path is indicated in fig. 5. In the following only the results for limb $l = 1$ are presented.

6.4.1 Inverse kinematics and constraint satisfaction

Application of Nested Algorithms 1 and 2: The inverse kinematics is solved for the trajectory sampled with time step size $\Delta t = 0.001$ s. Fig. 8 and Fig. 9a) show the trajectories of all tree-joint variables. The inverse kinematics problem of the limb along with the loop constraints for FC $\Lambda_{2(l)}$ are solved with the nested algorithms 1 and 2, respectively. The error threshold was set to $\epsilon = 10^{-10}$ in both algorithms. Fig. 10 shows the evolution of the error $\|\Delta \mathbf{x}_i\|$ of the inverse kinematics (algorithm 1) and the error $\|g\|$ of the cut-joint constraints of FC $\Lambda_{2(l)}$ (algorithm 2). The number of outer-loop iteration steps necessary for solving the limb inverse kinematics is shown in Fig. 11a). Between 1 and 3 iterations of the outer-loop (algorithm 1) are needed, which depends on the rate of change of the EE configuration and the corresponding generalized coordinates within one time step. The number of inner-loop iterations needed for solving the cut-joint constraints (algorithm 2) is shown in Fig. 12. Shown is the number of inner-loop iterations needed to solve the loop constraints within each particular outer-loop step for the inverse kinematics solution. From 1 to 3 inner-loop iterations are required to satisfy the constraints with the desired accuracy ϵ . The number of iterations depends on the rate of change of the tree-joint variable of the loop and the conditioning of the constraints. If the trajectory is sampled with a larger time step size of $\Delta t = 10^{-2}$ s, algorithm 1 needs 3 iterations almost all the time as shown in Fig. 11b). Then the error evolution is similar to that in Fig. 11 and 12.

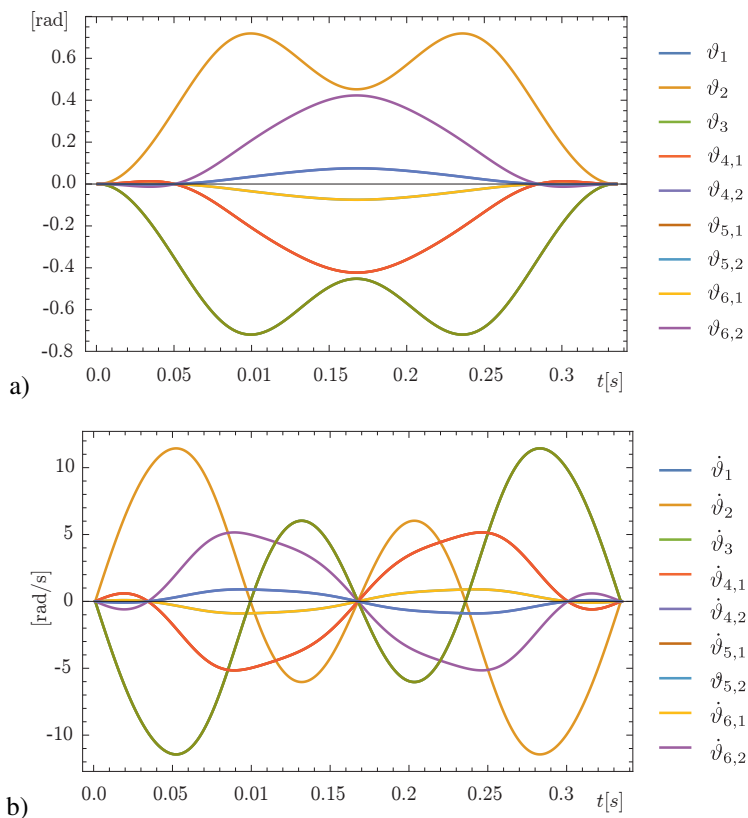


Fig. 8. Inverse kinematics solution for a) tree-joint angles, and b) velocities of limb $l = 1$.

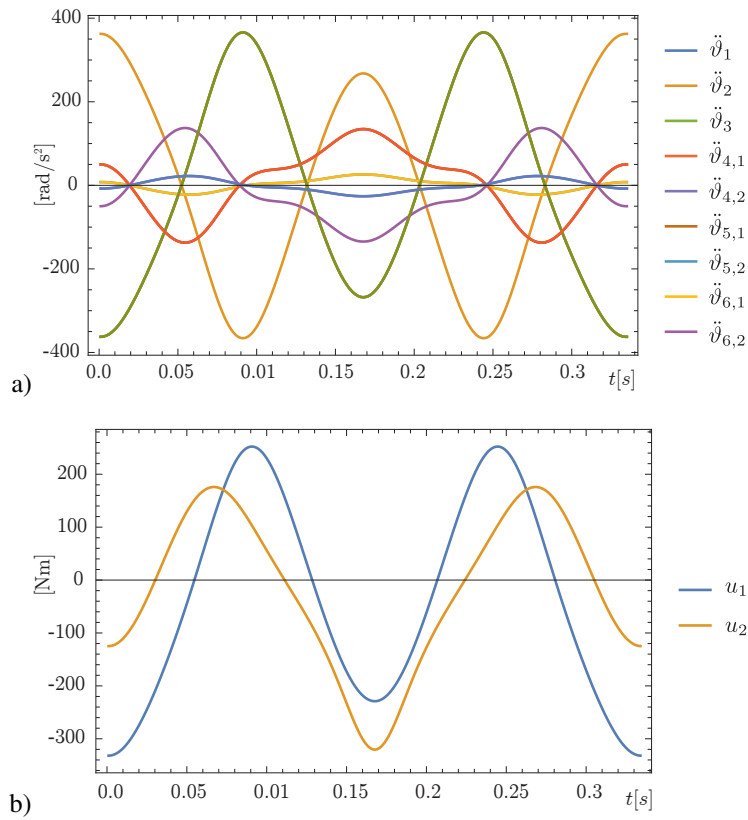


Fig. 9. a) Inverse kinematics solution for tree-joint accelerations of limb $l = 1$. b) Inverse dynamics solution (drive torques u_1 and u_2 at joint 1 of limb $l = 1$ and $l = 2$).

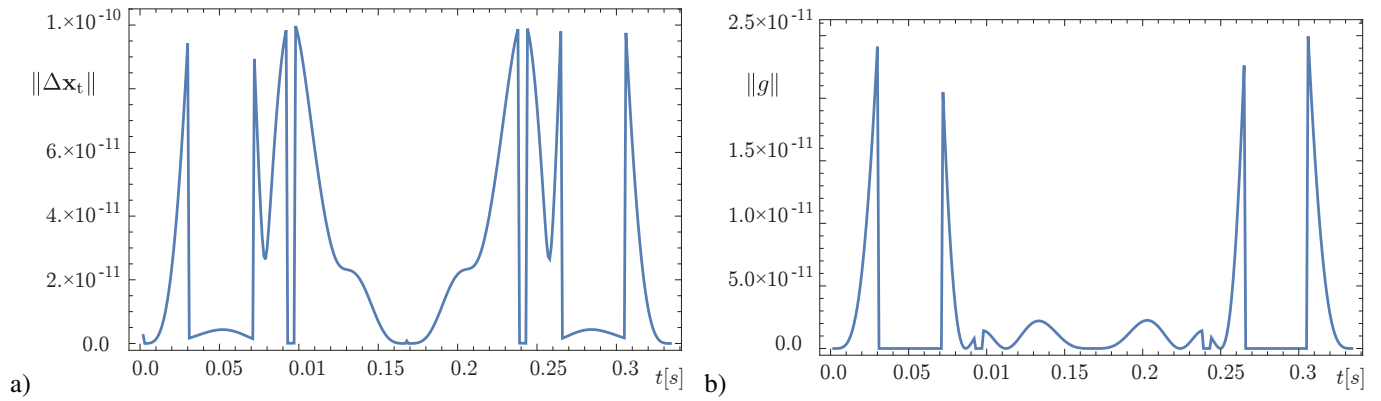


Fig. 10. a) Error of outer loop solving the inverse kinematics of limb, and b) of inner loop solving the loop constraints of FC $\Lambda_2(l)$.

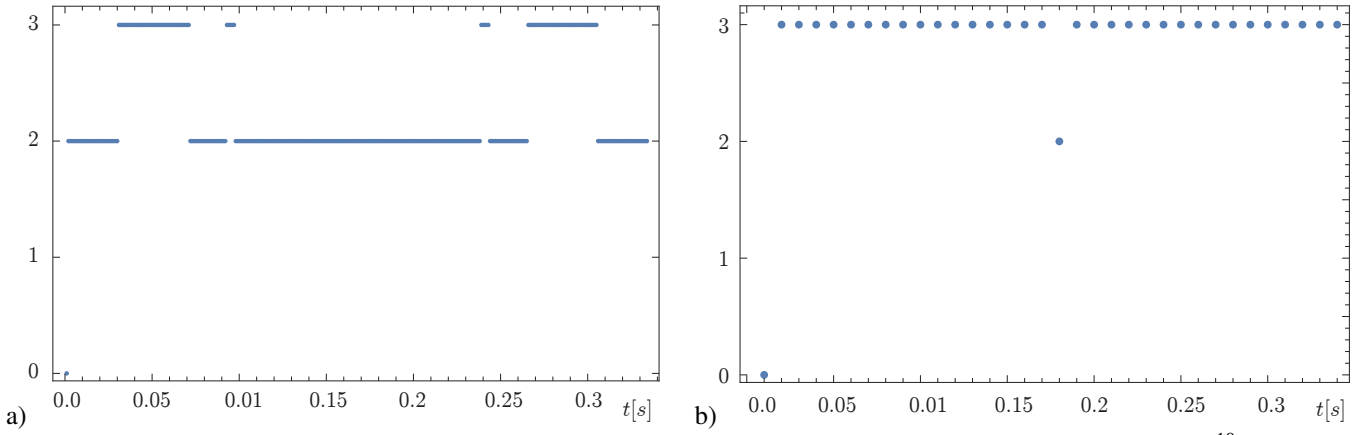


Fig. 11. Number of iterations required for solving the inverse kinematics of limb (algorithm 1) with precision goal $\varepsilon = 10^{-10}$, where a) $\Delta t = 0.001$ s, and b) $\Delta t = 0.01$ s.

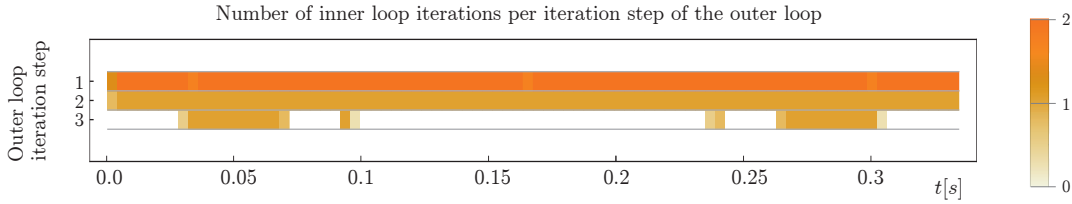


Fig. 12. Number of iterations required for solving the loop constraints for FC $\Lambda_{2(l)}$ (algorithm 2) within each iteration of algorithm 1 solving the inverse kinematics of limb with accuracy goal $\varepsilon = 10^{-10}$.

The Newton-Raphson scheme is known to have a quadratic convergence, and it is instructive to consider this for the inner- and outer-loop separately. As an example, the inverse kinematics is solved for a prescribed target position of the platform $\mathbf{r}_{6,0} + (0.2\text{m}, 0, 0.5\text{m})^T$, with initial configuration $\mathbf{r}_{6,0}$. The accuracy goal is $\varepsilon = 10^{-11}$ for both algorithms. The outer-loop needs 6 iterations to converge. Fig. 13a) shows the convergence of inverse kinematics error. The number of necessary iterations of the inner-loop differs for each step of the outer-loop. Fig. 13b) shows the number of inner-loop iteration cycles at each outer-loop step o . The corresponding convergence of the constraint error at each step o of the inverse kinematics outer-loop is shown in Fig. 14. In order to compare the convergence rate, the error $\|g\|$ is normalized relative to its initial value, i.e. shown is the error decay not its absolute value, which is always below ε after the last step. Step $i = 0$ refers to the initial value, where $\|g\| = 1$.

Application of Algorithm 3: Nesting algorithm 2 (inner-loop) with algorithm 1 (outer-loop) ensures that, at each outer-loop iteration step for solving the limb inverse kinematics, the constraints are satisfied with prescribed accuracy, which corresponds to numerically evaluating (23), i.e. the inverse of the combined map (21). This is crucial when the loop constraints are ill-conditioned. The loop constraints for FC $\Lambda_{2(l)}$ of the IRSBot-2 are well-conditioned, however, and there are no singularities within the used workspace. Separate numerical solution of the individual constraints is thus not necessary. Instead, both problems can be solved at once with algorithm 3 using a common iteration step. Fig. 15 shows the error evolution, and Fig. 16 the necessary number of iterations when algorithm 3 is applied with accuracy goal $\varepsilon = 10^{-10}$. The algorithm needs three iterations at almost every time step. The total number of iterations is almost the same as that needed by the nested algorithm, which in average needs two outer loop iteration steps with one and two inner loop iterations, respectively.

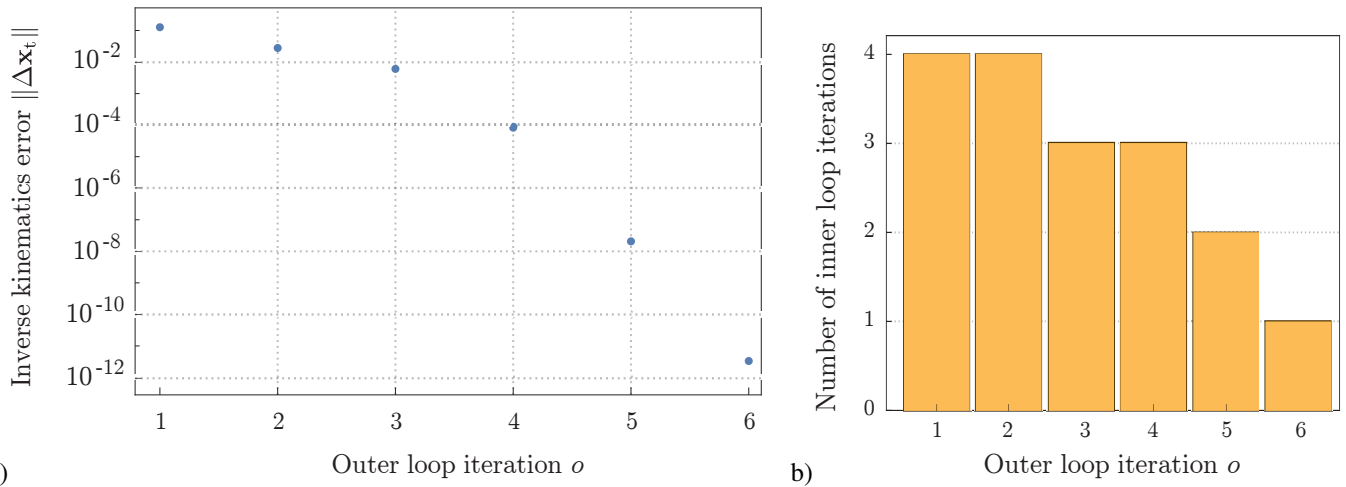


Fig. 13. a) Convergence of inverse kinematics error during outer-loop iterations. b) Number of inner-loop iterations required for solving the loop constraints of FC $\Lambda_2(t)$ at each iteration step of the outer-loop solving the inverse kinematics.

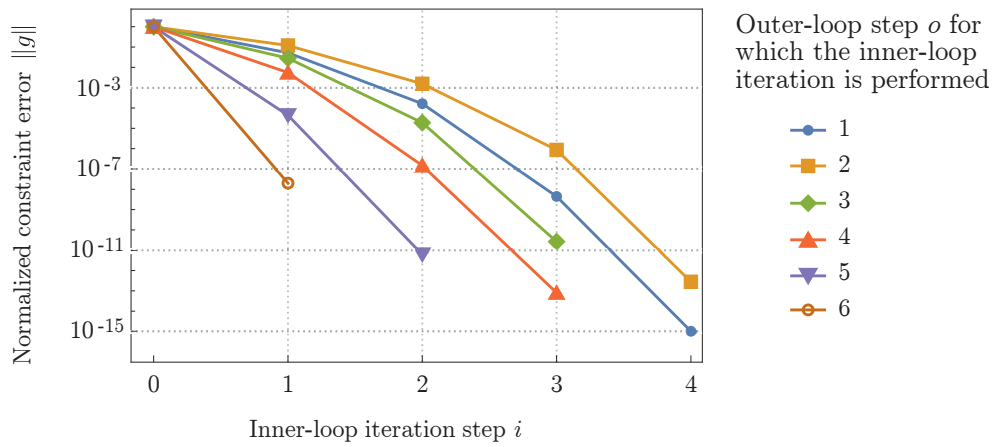


Fig. 14. Convergence of constraint error at each step of the outer-loop for solving the inverse kinematics of limb.

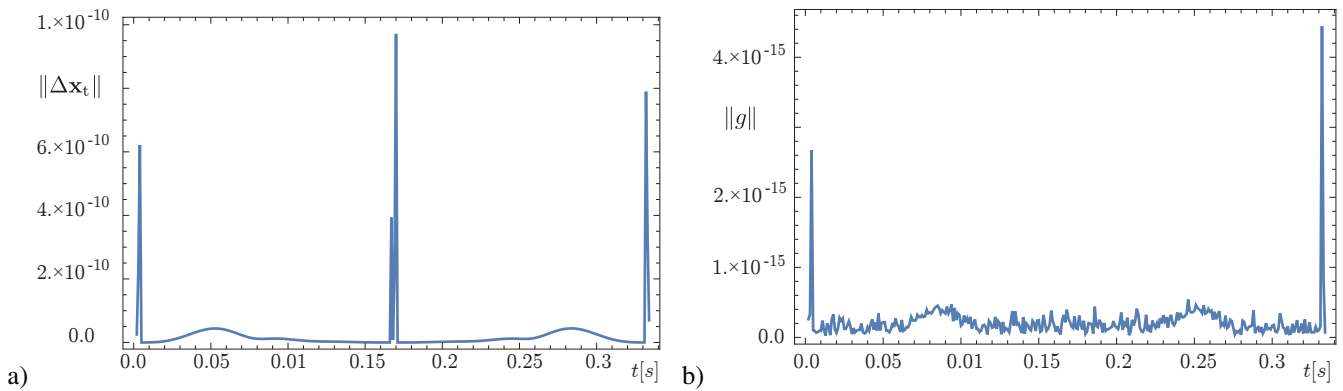


Fig. 15. Convergence of a) inverse kinematics and b) constraint error when using algorithm 3 for accuracy goal $\epsilon = 10^{-10}$.

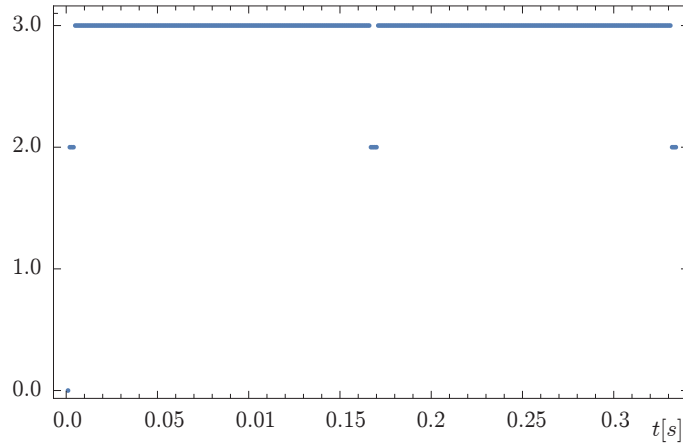


Fig. 16. Number of iterations required by algorithm 3 for accuracy goal $\epsilon = 10^{-10}$.

6.4.2 Inverse dynamics

The inverse dynamics solution (45) is evaluated for the joint trajectories $\vartheta_{(l)}(t), l = 1, 2$ obtained from the inverse kinematics solution, assuming no additional external forces other than gravity. The inertia properties of the links are estimated by modeling the bodies as geometric primitives. All bodies are assumed to be made of aluminum with homogenous mass distribution. Body 1 is modeled as a rigid beam with length $L_1 = 1/2$ m, and square cross section with side length $L_1/6$. Body 3 is a beam with length L_1 and side length $L_1/10$. Body 2 is simplified as a rectangular solid plate with side lengths $2(c_1 + d_1)$ and $2d_2$, and thickness $c_3 + d_3$. Links 4 and 5 are modeled as rigid beams with lengths $L_2 = 3/4$ m, and circular cross section with radius $L_2/30$. The platform is a solid rectangular plate with side lengths $4P_1$ and $3P_2$, and height $P_2/4$. A rendering of the model is shown in fig. 17. With the above numerical data, the mass m_i of body $i = 1, \dots, 5$ of each of the two identical limbs, and the platform $i = 6$ are $m_1 = 1.17188$ kg, $m_2 = 8.11899$ kg, $m_3 = 21.1875$ kg, $m_4 = m_5 = 1.1781$ kg, $m_6 = 1.97754$ kg. The inverse dynamics solution obtained by evaluating (45) is shown in Fig. 18, where u_1 and u_2 are the drive torques at joint 1 of limb $l = 1$ and $l = 2$, respectively. These are the feedforward control commands to be used model-based non-linear control schemes [3, 69, 70, 41].

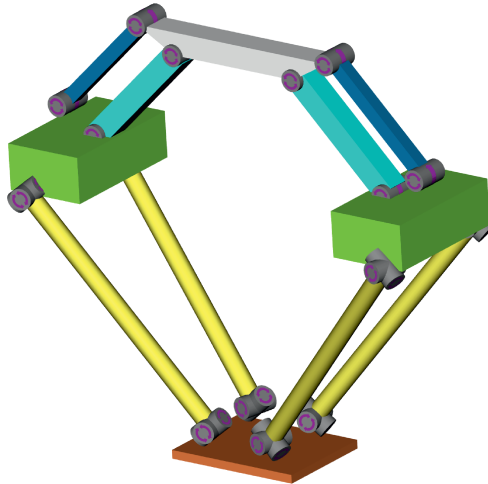


Fig. 17. Rendering of the dynamics model using geometric primitives.

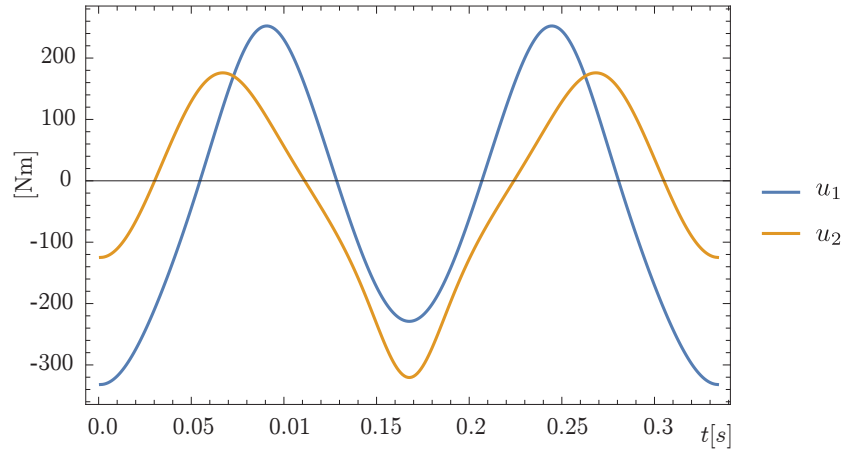


Fig. 18. Inverse dynamics solution: drive torque u_1 and u_2 at the actuated joint 1 of limb $l = 1, 2$.

6.4.3 Input Singularity

For completeness, the robustness of the proposed numerical solution scheme is investigated when the PKM passes near an input singularity (also called serial singularity [71]). To this end, the platform motion is prescribed as above with $\Delta x = -0.15$ m, $\Delta z = -0.6085$ m, which leads to limb 1 becoming stretched out at the inflection points of the platform trajectory. As a consequence, the task space Jacobian $\mathbf{L}_{t(l)}$ in (24), and thus $\mathbf{F}_{(l)}$ in (27), become ill-conditioned. The inverse kinematics solution is shown in Fig. 19. The closeness to the singularity causes a fast change in the motion direction of the limb leading to large accelerations. This is also visible in the inverse dynamics solution in Fig. 20a). The evolution of $\sqrt{\kappa(\mathbf{F}_{(l)}^T \mathbf{F}_{(l)})}$, where κ is the condition number, clearly indicates bad conditioning of the inverse kinematics Jacobian of the limb near the singularity (Fig. 20b). The necessary number of iterations of the inverse kinematics algorithm 1, shown in Fig. 21, is almost unaffected, however. Also the inner-loop needs at most two iterations to achieve the accuracy of $\epsilon = 10^{-10}$.

7 Conclusion

A local constraint embedding approach was presented for the modeling of PKM with complex loops, and incorporated into the task space formulation of EOM. The obtained model provides the basis for model-based non-linear control as well as for time simulation of the PKM dynamics. The constraint embedding along with the kinematic model of PKM can also be employed to perform kinematic simulations. For the numerical implementation of the constraint embedding method, a nested Newton-Raphson algorithm 1 is proposed, which iteratively solves the inverse kinematics of a limb making use of the iterative solution of the inner-limb loop constraints (algorithm 2). This admits dealing with redundant (or general ill-conditioned) inner-loop constraints. The latter occur for several PKM of practical relevance. A good example is the 3R[2UU] Delta robot, where each limb contains a single loop modeled as a 4U loop. For this 4U loop, four constraints introduced, but only three of them are independent. This redundancy can be dealt with for each of the individual loops in algorithm 2. This is an advantage of the proposed local constraint embedding strategy, and a clear advantage over the standard MBS formulation. If the individual constraints are regular, as in case of the IRSBot-2 example, the loop constraints can be solved along with the limb inverse kinematics constraints with algorithm 3. An important aspect of the introduced formulation is that the intra-limb constraint, the inverse kinematics problem, and the EOM (34) of the tree-topology system can be solved and evaluated independently. This allows for parallel computation in order to increase the computational efficiency. The formulation or algorithm for evaluating the EOM (34) is arbitrary. If appropriate, they can be evaluated with recursive $O(n)$ -algorithm so to further improve the efficiency. A method that is efficient and easy to use at the same time is the Lie group formulation for EOM in closed form [65, 50, 46] and for the recursive algorithm [46, 72, 66]. Future research will address adoption of the modular modeling concept [60, 24] to the constraint embedding.

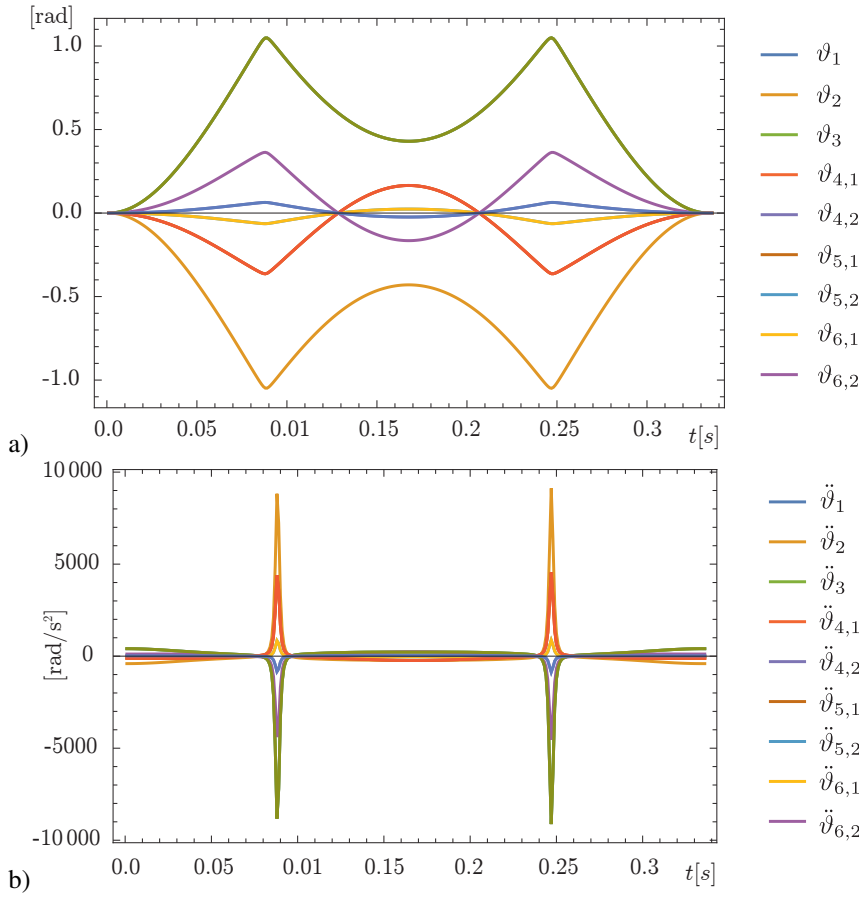


Fig. 19. a) Tree-joint variables according to the EE-trajectory passing near an input singularity. b) The corresponding tree-joint accelerations.

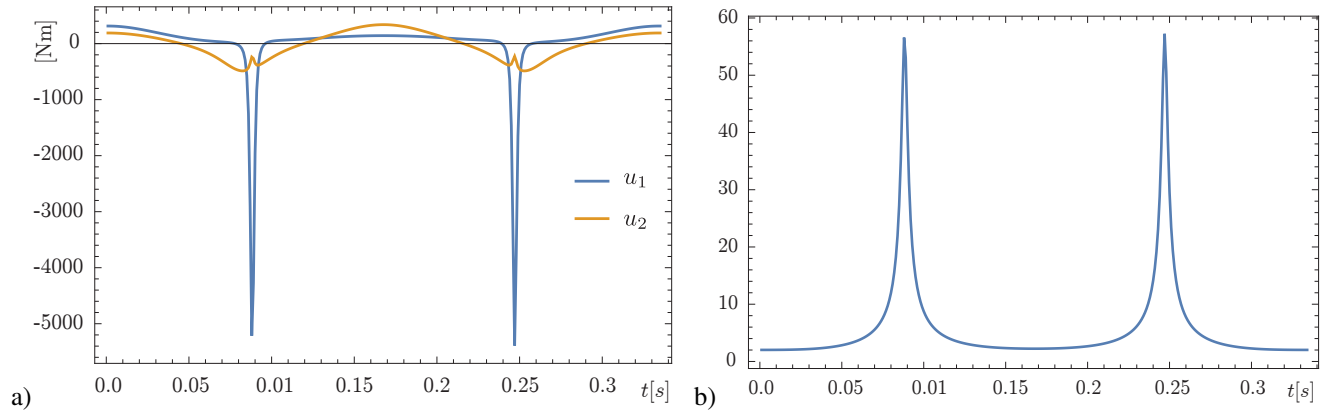


Fig. 20. a) Inverse dynamics solution (drive torques u_1 and u_2) for the EE-trajectory passing an input singularity. b) Time evolution of $\sqrt{\kappa(\mathbf{F}_{(l)}^T \mathbf{F}_{(l)})}$ along that trajectory.

A Cut-Joint Constraints

The cut-joint formulation is well-known in computational multibody system dynamics [52, 73, 8]. This is summarized in the following in a form compatible with the presented formulation. A joint with DOF δ imposes $m_{\lambda,l} = 6 - \delta$ constraints, e.g., a revolute joint imposes $m_{\lambda,l} = 5$, a spherical (ball-socket) joint imposes $m_{\lambda,l} = 3$, and a universal/hook joint imposes $m_{\lambda,l} = 4$ constraints. The specific cut-joint constraints are available for all technical joints. The particular constraints are obtained by combining *elementary constraints*, i.e. constraints on the relative translation and rotation of interconnected body.

Notice that in special situations, the system of $m_{\lambda,l}$ constraints for loop $\Lambda_{\lambda(l)}$ may be redundant. Possible redundancy of the overall system of m_l intra-limb constraints for limb l , or of the overall system of m constraints that would be imposed to the PKM model in the standard MBS modeling approach, is not an issue for the local constraint embedding method.

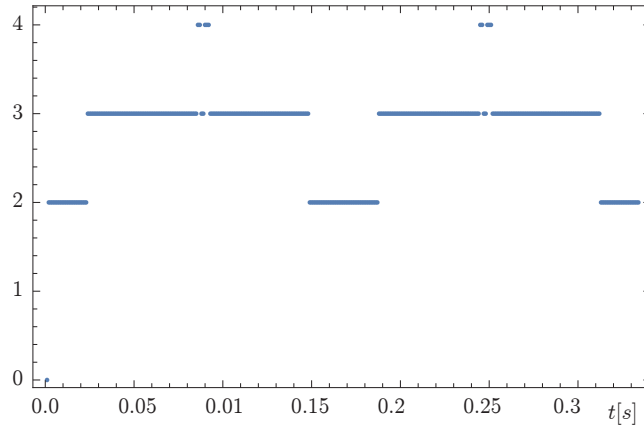


Fig. 21. Number of iterations needed by the outer-loop algorithm 1 to solve the limb inverse kinematics with a precision goal $\varepsilon = 10^{-10}$.

A.1 Elementary Cut-Joint Constraints

The cut-joint of FC $\Lambda_{\lambda(l)}$ connects body k and r of limb l . Denote with $\mathcal{F}_{k(l)}$ and $\mathcal{F}_{r(l)}$ the body-fixed frame on body k and r , and with $\mathbf{R}_{k(l)}$ and $\mathbf{R}_{r(l)}$ the absolute rotation matrix of $\mathcal{F}_{k(l)}$ and $\mathcal{F}_{r(l)}$ relative to the IFR, respectively (Fig. 22a). They, and the absolute position vectors \mathbf{r}_k and \mathbf{r}_r are known from the absolute configurations \mathbf{C}_k and \mathbf{C}_r . In the following, the index (l) is omitted as all derivations refer to limb l . The rotation matrix of body r relative to body k is thus $\mathbf{R}_{k,r} := \mathbf{R}_k^T \mathbf{R}_r$. Let ${}^k \mathbf{d}_{k,\lambda}$ and ${}^r \mathbf{d}_{r,\lambda}$ be the constant position vector of the reference point of the cut-joint (e.g. rotation center of spherical or universal joints, point at joint axis of revolute or cylindrical joints) measured in frame k and r , respectively. The velocity and acceleration constraints restrict the velocities $\mathbf{V}_{r(l)}$, $\mathbf{V}_{k(l)}$ and accelerations $\dot{\mathbf{V}}_{r(l)}$, $\dot{\mathbf{V}}_{k(l)}$ of the two bodies. They are expressed in terms of $\dot{\vartheta}_{(\lambda,l)}$, $\ddot{\vartheta}_{(\lambda,l)}$ using the geometric Jacobian. In the following explicit relations for general constraints are presented that are suited for PKM modeling. The difference to the formulation used in MBS dynamics is that no dedicated cut-joint frames are introduced.

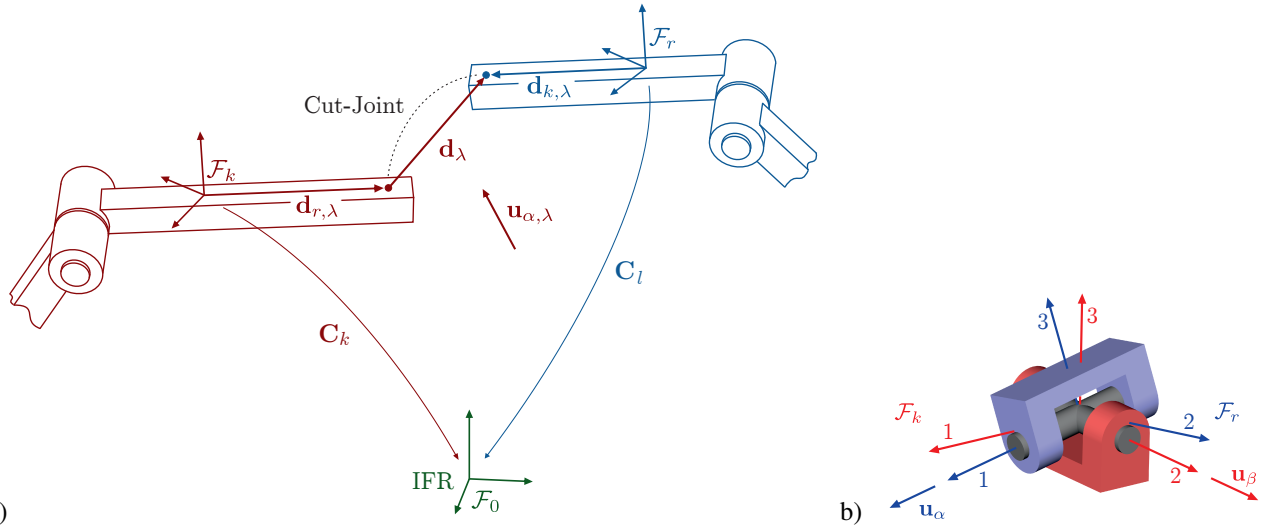


Fig. 22. a) Generic definition of cut-joint geometry. b) Definition of two vectors \mathbf{u}_α and \mathbf{u}_β for defining the orientation constraint of a U joint. The condition is that they remain perpendicular.

Distance constraints: The relative translation of the reference point of the cut-joint at body k and r , respectively, expressed in \mathcal{F}_k is

$${}^k \mathbf{d}_\lambda = {}^k \mathbf{d}_{r,\lambda} - {}^k \mathbf{d}_{k,\lambda} + {}^k \mathbf{r}_r - {}^k \mathbf{r}_k \quad (50)$$

with ${}^k \mathbf{d}_{r,\lambda} = \mathbf{R}_{k,r} {}^r \mathbf{d}_{r,\lambda}$ and ${}^k \mathbf{r}_r = \mathbf{R}_k^T \mathbf{r}_r$, ${}^k \mathbf{r}_k = \mathbf{R}_k^T \mathbf{r}_k$ (Fig. 22a). This relative translation is restricted in certain directions, according to the cut-joint. Denote with ${}^k \mathbf{u}_{\alpha,\lambda(l)}$ unit vectors along relative translations that are prohibited by the cut-joint.

The elementary displacement constraint is thus $g_{\alpha,\lambda}^{\text{pos}} = 0$, where

$$g_{\alpha,\lambda}^{\text{pos}} := {}^k \mathbf{u}_{\alpha,\lambda}^T {}^k \mathbf{d}_\lambda. \quad (51)$$

The relative configuration of the bodies depends on the joint variables of the FC $\Lambda_{\lambda(l)}$ only, and thus $g_{\alpha,\lambda}^{\text{pos}} = g_{\alpha,\lambda}^{\text{pos}}(\boldsymbol{\vartheta}_{(\lambda,l)})$.

Using $\dot{\mathbf{R}}_{k,r} = \mathbf{R}_{k,r} {}^r \tilde{\boldsymbol{\omega}}_r - {}^k \tilde{\boldsymbol{\omega}}_k \mathbf{R}_{k,r}$, the relative velocity and acceleration of body k and r can be expressed as

$${}^k \dot{\mathbf{d}}_\lambda = \mathbf{A}_\lambda \dot{\boldsymbol{\vartheta}}_{(\lambda,l)} = \mathbf{B}_\lambda \begin{pmatrix} \mathbf{V}_k \\ \mathbf{V}_r \end{pmatrix} \quad (52)$$

$${}^k \ddot{\mathbf{d}}_\lambda = \mathbf{A}_\lambda \ddot{\boldsymbol{\vartheta}}_{(\lambda,l)} + \dot{\mathbf{A}}_\lambda \dot{\boldsymbol{\vartheta}}_{(\lambda,l)} = \mathbf{B}_\lambda \begin{pmatrix} \dot{\mathbf{V}}_k \\ \dot{\mathbf{V}}_r \end{pmatrix} + \dot{\mathbf{B}}_\lambda \begin{pmatrix} \mathbf{V}_k \\ \mathbf{V}_r \end{pmatrix} \quad (53)$$

with

$$\mathbf{A}_\lambda := \mathbf{B}_\lambda \mathbf{J}_\lambda \quad (54)$$

$$\dot{\mathbf{A}}_\lambda = \mathbf{B}_\lambda \dot{\mathbf{J}}_\lambda + \dot{\mathbf{B}}_\lambda \mathbf{J}_\lambda$$

$$\begin{aligned} \mathbf{B}_\lambda &:= \begin{pmatrix} {}^k \mathbf{d}_\lambda + {}^k \tilde{\mathbf{d}}_{r,\lambda} - \mathbf{I} & -{}^k \tilde{\mathbf{d}}_{r,\lambda} \mathbf{R}_{k,r} \end{pmatrix} \\ \dot{\mathbf{B}}_\lambda &= \begin{pmatrix} {}^k \dot{\mathbf{d}}_\lambda & \mathbf{0} & ({}^k \tilde{\boldsymbol{\omega}}_r - {}^k \tilde{\boldsymbol{\omega}}_k) {}^k \tilde{\mathbf{d}}_{r,\lambda} \mathbf{R}_{k,r} & ({}^k \tilde{\boldsymbol{\omega}}_r - {}^k \tilde{\boldsymbol{\omega}}_k) \mathbf{R}_{k,r} \end{pmatrix} \\ \mathbf{J}_\lambda &:= \begin{pmatrix} \mathbf{J}_{k,\lambda} \\ \mathbf{J}_{r,\lambda} \end{pmatrix} \end{aligned} \quad (55)$$

where $\mathbf{J}_{k,\lambda(l)}$ and $\mathbf{J}_{r,\lambda(l)}$ are the submatrices of the Jacobians $\mathbf{J}_{k(l)}$ and $\mathbf{J}_{r(l)}$ of body k and r , respectively, with the $n_{\lambda,l}$ columns corresponding to the joint variables of FC $\Lambda_{(l)}^k$, and $\boldsymbol{\omega}_r = \mathbf{R}_{k,r} {}^r \boldsymbol{\omega}_r$. The Jacobians and their time derivatives are given in (6) and (9). The velocity and acceleration constraints are thus $\dot{g}_{\alpha,\lambda}^{\text{pos}} = 0$ and $\ddot{g}_{\alpha,\lambda}^{\text{pos}} = 0$, with

$$\dot{g}_{\alpha,\lambda}^{\text{pos}} := {}^k \mathbf{u}_{\alpha,\lambda}^T {}^k \dot{\mathbf{d}}_\lambda = {}^k \mathbf{u}_{\alpha,\lambda}^T \mathbf{A}_\lambda \dot{\boldsymbol{\vartheta}}_{(\lambda,l)} \quad (56)$$

$$\ddot{g}_{\alpha,\lambda}^{\text{pos}} := {}^k \mathbf{u}_{\alpha,\lambda}^T {}^k \ddot{\mathbf{d}}_\lambda = {}^k \mathbf{u}_{\alpha,\lambda}^T \mathbf{A}_\lambda \ddot{\boldsymbol{\vartheta}}_{(\lambda,l)} + {}^k \mathbf{u}_{\alpha,\lambda}^T \dot{\mathbf{A}}_\lambda \dot{\boldsymbol{\vartheta}}_{(\lambda,l)}. \quad (57)$$

Orientation constraints: A constraint on the relative orientation of the two bodies is described by the condition that the angle between a vector ${}^k \mathbf{u}_\alpha$ fixed on body k and a vector ${}^r \mathbf{u}_\beta$ fixed at body r remains constant. The particular (and most relevant) situation that these two vectors are perpendicular is expressed by the constraint $g_{\alpha,\beta}^{\text{rot}} = 0$, where

$$g_{\alpha,\beta}^{\text{rot}} := {}^k \mathbf{u}_\alpha^T \mathbf{R}_{k,r} {}^r \mathbf{u}_\beta = {}^r \mathbf{u}_\alpha^T {}^k \mathbf{u}_\beta \quad (58)$$

and ${}^k \mathbf{u}_\beta = \mathbf{R}_{k,r} {}^r \mathbf{u}_\beta$. Fig. 22b) shows this for a U joint. The corresponding velocity constraints are $\dot{g}_{\alpha,\beta}^{\text{rot}}(\boldsymbol{\vartheta}_{(\lambda,l)}, \dot{\boldsymbol{\vartheta}}_{(\lambda,l)}) = 0$ and $\ddot{g}_{\alpha,\beta}^{\text{rot}}(\boldsymbol{\vartheta}_{(\lambda,l)}, \dot{\boldsymbol{\vartheta}}_{(\lambda,l)}, \ddot{\boldsymbol{\vartheta}}_{(\lambda,l)}) = 0$, with

$$\dot{g}_{\alpha,\beta}^{\text{rot}} = {}^k \mathbf{u}_\alpha^T \dot{\mathbf{A}}_{\beta}^{\text{rot}} \dot{\boldsymbol{\vartheta}}_{(\lambda,l)} \quad (59)$$

$$\ddot{g}_{\alpha,\beta}^{\text{rot}} = {}^k \mathbf{u}_\alpha^T \ddot{\mathbf{A}}_{\beta}^{\text{rot}} \dot{\boldsymbol{\vartheta}}_{(\lambda,l)} + {}^k \mathbf{u}_\alpha^T \dot{\mathbf{A}}_{\beta}^{\text{rot}} \ddot{\boldsymbol{\vartheta}}_{(\lambda,l)} \quad (60)$$

with $\mathbf{A}_\beta^{\text{rot}} := \mathbf{B}_\beta^{\text{rot}} \mathbf{J}_\lambda$ and $\dot{\mathbf{A}}_\beta^{\text{rot}} = \mathbf{B}_\beta^{\text{rot}} \dot{\mathbf{J}}_\lambda + \dot{\mathbf{B}}_\beta^{\text{rot}} \mathbf{J}_\lambda$, where

$$\begin{aligned} \mathbf{B}_\beta^{\text{rot}} &:= \begin{pmatrix} {}^k \tilde{\mathbf{u}}_\beta & \mathbf{0} & -\mathbf{R}_{k,r} {}^r \tilde{\mathbf{u}}_\beta & \mathbf{0} \end{pmatrix} \\ \dot{\mathbf{B}}_\beta^{\text{rot}} &= - \begin{pmatrix} \tilde{\mathbf{c}} & \mathbf{0} & ({}^k \tilde{\boldsymbol{\omega}}_k - {}^k \tilde{\boldsymbol{\omega}}_r) {}^k \tilde{\mathbf{u}}_\beta \mathbf{R}_{k,r} & \mathbf{0} \end{pmatrix} \end{aligned}$$

abbreviating $\mathbf{c} := {}^k \tilde{\mathbf{u}}_\beta ({}^k \boldsymbol{\omega}_k - {}^k \boldsymbol{\omega}_r)$. In the expression $\dot{\mathbf{B}}_\beta^{\text{rot}} \mathbf{J}_\lambda \dot{\vartheta}_{(\lambda,l)}$, matrix $\dot{\mathbf{B}}_\beta^{\text{rot}}$ can be replaced by

$$\bar{\mathbf{B}}_\beta^{\text{rot}} := - \begin{pmatrix} {}^k \tilde{\boldsymbol{\omega}}_k {}^k \tilde{\mathbf{u}}_\beta & \mathbf{0} & ({}^k \tilde{\boldsymbol{\omega}}_r - 2{}^k \tilde{\boldsymbol{\omega}}_k) {}^k \tilde{\mathbf{u}}_\beta \mathbf{R}_{k,r} & \mathbf{0} \end{pmatrix}$$

which may be computationally advantageous (notice that $\bar{\mathbf{B}}_\beta^{\text{rot}}$ is not the time derivative of $\mathbf{B}_\beta^{\text{rot}}$).

A.2 Constraints for Technical Joints

Joint specific constraints are introduced by combining the above elementary constraints. The geometric constraints (12) are formed by the corresponding position and orientation constraints determined by (51) and (58). The rows of the constraint Jacobian $\mathbf{G}_{(\lambda,l)}$ of the velocity constraints (13) are ${}^k \mathbf{u}_{\alpha,\lambda}^T \mathbf{A}_\lambda$ (56), for the position constraints, and ${}^k \mathbf{u}_\alpha^T \mathbf{A}_\beta^{\text{rot}}$ in (59) for rotation constraints. The rows of $\dot{\mathbf{G}}_{(\lambda,l)}$ in (14) are ${}^k \mathbf{u}_{\alpha,\lambda}^T \dot{\mathbf{A}}_\lambda$ in (57), and ${}^k \mathbf{u}_\alpha^T \dot{\mathbf{A}}_\beta^{\text{rot}}$ in (60).

Revolute, spherical, and universal joints, for instance, do not permit relative displacements, and ${}^k \mathbf{d}_\lambda$ must vanish. Then (12) comprises the three translation constraints $g_\alpha^{\text{pos}} = 0, \alpha = 1, 2, 3$

$$\mathbf{g}_{(\lambda,l)} = (g_1^{\text{pos}}, g_2^{\text{pos}}, g_3^{\text{pos}})^T := {}^k \mathbf{d}_\lambda. \quad (61)$$

Prismatic and cylindrical joints allow for translation along an axis. Denote with ${}^k \mathbf{u}_{\alpha,\lambda}, \alpha = 1, 2$ independent unit vectors perpendicular to this axis. The two position constraints $g_\alpha^{\text{pos}} = 0, \alpha = 1, 2$ are then defined by (51), and $\mathbf{g}_{(\lambda,l)} = (g_1^{\text{pos}}, g_2^{\text{pos}})^T$. A joint with δ^{rot} rotary DOFs imposes $3 - \delta^{\text{rot}}$ such orientation constraints (58).

B List of Symbols

n_l	- number of tree-joints in limb l
L	- number of (complex) limbs
$\Gamma^{(l)}$	- topological graph of limb $l = 1, \dots, L$
$\Lambda_{\lambda^{(l)}}$	- FC $\lambda = 1, \dots, \gamma_l$ of limb l
γ_l	- number of FCs of $\Gamma^{(l)}$, number of loops in limb l
n	- number of joint variables of the tree-topology system according to \bar{G}
n_l	- number of tree-joint variables of limb l
$n_{\lambda,l}$	- number of tree-joint variables of limb l when the platform is removed
$\bar{n} := \bar{n}_1 + \dots + \bar{n}_L$	- total number of variables of the tree-topology system when the platform is removed
\underline{k}	- index of the last body in the path from body k to the ground, i.e. $0 = \underline{k} - 1$
λ	- cut-edge of Λ_l . It serves as start edge when traversing the FC.
$\bar{\lambda}$	- last edge when traversing the FC starting from λ
$m_{\lambda,l}$	- number of independent loop constraints of FC λ of limb l
$\delta_{0,l}$	- number of joint variables of limb l that are not part of a FC of $\Gamma^{(l)}$
$\delta_{\lambda,l} = n_{\lambda,l} - m_{\lambda,l}$	- DOF of FC λ of limb l when disconnected from the platform
$\delta_l = \delta_{0,l} + \delta_{1,l} + \dots + \delta_{\gamma_l,l}$	- DOF of limb l when disconnected from the platform
$\delta_{p^{(l)}}$	- platform DOF of separated limb l
δ_p	- platform DOF of PKM
$\vartheta^{(l)} \in \mathbb{V}^{n_l}$	- vector of tree-joint variables $\vartheta_1, \dots, \vartheta_{n_l}$ of limb l (when connected to platform)
$\bar{\vartheta}^{(l)} \in \mathbb{V}^{\bar{n}_l}$	- vector of tree-joint variables $\vartheta_1, \dots, \vartheta_{\bar{n}_l}$ of limb l (when disconnected from platform)
ϑ_{act}	- vector of actuated joint coordinates
$\mathbf{q}^{(\lambda,l)}$	- vector of $\delta_{\lambda,l}$ independent variables used to express the solution the loop constraints for $\Lambda_{(\lambda,l)}$
$\mathbf{q}^{(l)}$	- vector of δ_l generalized coordinates of limb l when separated from PKM
$\Phi_{p^{(l)}}$	- forward kinematics map of limb l , so that $\mathbf{C}_{p^{(l)}}(\vartheta^{(l)}) = \Phi_{p^{(l)}}(\mathbf{q}^{(l)})$
$f^{(l)}$	- inverse kinematics map of limb l , so that $\mathbf{q}^{(l)} = f^{(l)}(\mathbf{C}_p)$
$\mathbf{L}_{t^{(l)}}$	- task space Jacobian of limb l , so that $\mathbf{V}_t = \mathbf{L}_{t^{(l)}}\dot{\mathbf{q}}^{(l)}$
$\mathbf{F}^{(l)}$	- inverse kinematics Jacobian of limb l , so that $\mathbf{V}_{p^{(l)}} = \mathbf{L}_{p^{(l)}}\dot{\mathbf{q}}^{(l)}$
$\tilde{\mathbf{x}} = \begin{pmatrix} 0 & -x_3 & x_2 \\ x_3 & 0 & -x_1 \\ -x_2 & x_1 & 0 \end{pmatrix} \in so(3)$	- $\mathbf{x} = \begin{pmatrix} x_1 \\ x_2 \\ x_3 \end{pmatrix} \in \mathbb{R}^3$
$\hat{\mathbf{X}} = \begin{pmatrix} \tilde{\mathbf{x}} & \mathbf{y} \\ \mathbf{0} & 0 \end{pmatrix} \in se(3)$	- $\mathbf{X} = \begin{pmatrix} \mathbf{x} \\ \mathbf{y} \end{pmatrix} \in \mathbb{R}^6, \mathbf{x}, \mathbf{y} \in \mathbb{R}^3$
$\mathbf{Y}_i = (\mathbf{e}_i, \mathbf{y}_i \times \mathbf{e}_i + h_i \mathbf{e}_i)^T$	- Screw coordinate vector of joint i , $\mathbf{e}_i \in \mathbb{R}^3$ is a unit vector along the joint axis, $\mathbf{y}_i \in \mathbb{R}^3$ is the position vector to a point on the axis, $h_i \in \mathbb{R}^+$ is the pitch of the joint.
$\mathbf{Y}_i = (\mathbf{e}_i, \mathbf{y}_i \times \mathbf{e}_i)^T$	- Screw coordinate vector for a revolute joint
$\mathbf{Y}_i = (\mathbf{0}, \mathbf{e}_i)^T$	- Screw coordinate vector for a prismatic joint
$\mathbf{C}_i \in SE(3)$	- absolute configuration of body i w.r.t. to IFR
$\mathbf{C}_{i,j} := \mathbf{C}_i^{-1} \mathbf{C}_j \in SE(3)$	- relative configuration of body j relative to body i
$\mathbf{Ad}_{\mathbf{C}} = \begin{pmatrix} \mathbf{R} & \mathbf{0} \\ \tilde{\mathbf{r}} \mathbf{R} & \mathbf{R} \end{pmatrix}$	- Adjoint operator, so that $\mathbf{Y}^1 = \mathbf{Ad}_{\mathbf{C}_{12}} \mathbf{Y}^2$ is the transformation of screw coordinates represented in frame 1 to those represented in frame 2
$\mathbf{ad}_{\mathbf{x}} = \begin{pmatrix} \tilde{\xi} & \mathbf{0} \\ \tilde{\eta} & \tilde{\xi} \end{pmatrix}$	- Matrix form of the adjoint operator, so that $\mathbf{ad}_{\mathbf{Y}_1} \mathbf{Y}_2$ is the Lie bracket (screw product) of two screw coordinate vectors $\mathbf{Y}_1 = (\xi_1, \eta_1)^T$ and $\mathbf{Y}_2 = (\xi_2, \eta_2)^T$.
FC	- Fundamental Cycle (a topologically independent loop) of the topological graph
EE	- End-Effector
IFR	- Inertial Frame

Acknowledgement

This work has been supported by the LCM K2 Center for Symbiotic Mechatronics within the framework of the Austrian COMET-K2 program.

References

- [1] G. Rodriguez, "Kalman filtering, smoothing, and recursive robot arm forward and inverse dynamics," *IEEE Journal on Robotics and Automation*, vol. 3, no. 6, pp. 624–639, December 1987.
- [2] J. Wittenburg, *Dynamics of Multibody Systems*, 2nd ed. Springer, 2008.
- [3] J. Angeles, *Fundamentals of robotic mechanical systems*, 3rd ed. Springer, 2007.
- [4] M. Thomas and D. Tesar, "Dynamic modeling of serial manipulator arms," *ASME J. Dynamic Systems, Measurement, and Control*, vol. 104, pp. 218–228, 1982.
- [5] W. Stelzle, A. Kecskeméthy, and M. Hiller, "A comparative study of recursive methods," *Archive of applied mechanics*, vol. 66, no. 1, pp. 9–19, 1995.
- [6] R. Featherstone, *Rigid Body Dynamics Algorithms*. Springer, 2008.
- [7] K. Yamane and Y. Nakamura, "Comparative study on serial and parallel forward dynamics algorithms for kinematic chains," *The International Journal of Robotics Research*, vol. 28, no. 5, pp. 622–629, 2009.
- [8] A. A. Shabana, *Dynamics of Multibody Systems*, 4th ed. Cambridge University Press, 2013.
- [9] A. Jain, *Robot and Multibody Dynamics*. Springer US, 2011.
- [10] J. D. Jalon, J. Unda, and A. Avello, "Natural coordinates for the computer analysis of multibody systems," *Computer Methods in Applied Mechanics and Engineering*, vol. 56, no. 3, pp. 309–327, 1986.
- [11] J. G. de Jalon and E. Bayo, *Kinematic and Dynamic Simulation of Multibody Systems: The Real Time Challenge*. Berlin, Heidelberg: Springer, 1994.
- [12] K. Lee and D. Shah, "Dynamic analysis of a three-degrees-of-freedom in-parallel actuated manipulator," *IEEE Journal on Robotics and Automation*, vol. 4, no. 3, pp. 361–367, June 1988.
- [13] Y. Nakamura and M. Ghodoussi, "Dynamics computation of closed-link robot mechanisms with nonredundant and redundant actuators," *IEEE Transactions on Robotics and Automation*, vol. 5, no. 3, pp. 294–302, June 1989.
- [14] V. Mata, S. Provenzano, J. Cuadrado, and F. Valero, "Inverse dynamic problem in robots using gibbs-appell equations," *Robotica*, vol. 20, no. 1, pp. 59–67, 2002.
- [15] E. Abedloo, A. Molaei, and H. D. Taghirad, "Closed-form dynamic formulation of spherical parallel manipulators by gibbs-appell method," in *RSI/ISM International Conference on Robotics and Mechatronics, Tehran, Iran, October 15-17 2014*, pp. 576–581.
- [16] A. Müller, "Internal preload control of redundantly actuated parallel manipulators –its application to backlash avoiding control," *IEEE Trans. Robotics*, vol. 21, no. 4, pp. 668–677, 2005.
- [17] B. Dasgupta and T. Mruthyunjaya, "A Newton-Euler formulation for the inverse dynamics of the Stewart platform manipulator," *Mechanism and Machine Theory*, vol. 33, no. 8, pp. 1135 – 1152, 1998.
- [18] J. Wang and C. M. Gosselin, "A new approach for the dynamic analysis of parallel manipulators," *Multibody System Dynamics*, vol. 2, no. 3, pp. 317–334, Sep 1998.
- [19] J. Zhao, F. Chu, and Z. Feng, "Kinematics of spatial parallel manipulators with tetrahedron coordinates," *IEEE Transactions on Robotics*, vol. 30, no. 1, pp. 233–243, Feb 2014.
- [20] A. Müller, "Motion equations in redundant coordinates with application to inverse dynamics of constrained mechanical systems," *Nonlinear Dynamics*, vol. 67, no. 4, pp. 2527–2541, 2012.
- [21] A. Müller and T. Hufnagel, "Model-based control of redundantly actuated parallel manipulators in redundant coordinates," *Robotics and Autonomous systems*, vol. 60, no. 4, pp. 563–571, 2012.
- [22] W. Khalil and O. Ibrahim, "General solution for the dynamic modeling of parallel robots," *Journal of intelligent and robotic systems*, vol. 49, no. 1, pp. 19–37, 2007.
- [23] C. Gosselin, "Gravity compensation, static balancing and dynamic balancing of parallel mechanisms," in *Smart devices and machines for advanced manufacturing*. Springer, 2008, pp. 27–48.
- [24] A. Müller, "Dynamics of parallel manipulators with hybrid complex limbs —Modular modeling and parallel computing," *Mechanism and Machine Theory*, vol. 167, p. 104549 (36 pages), 2022.
- [25] W. Khalil and S. Guegan, "Inverse and direct dynamic modeling of gough-stewart robots," *IEEE Transactions on Robotics*, vol. 20, no. 4, pp. 754–761, 2004.
- [26] S. Briot and W. Khalil, *Dynamics of Parallel Robots*. Springer, 2015.
- [27] H. Abdellatif and B. Heimann, "Computational efficient inverse dynamics of 6-DOF fully parallel manipulators by using the Lagrangian formalism," *Mechanism and Machine Theory*, vol. 44, no. 1, pp. 192 – 207, 2009.
- [28] A. Jain, "Recursive algorithms using local constraint embedding for multibody system dynamics," in *International Design Engineering Technical Conferences and Computers and Information in Engineering Conference*, vol. 49019, 2009, pp. 139–147.
- [29] ———, "Multibody graph transformations and analysis," *Nonlinear Dyn*, vol. 67, pp. 2153–2170, 2012.
- [30] A. Jain, C. Crean, C. Kuo, and M. B. Quadrelli, "Efficient constraint modeling for closed-chain dynamics," in *The 2nd Joint International Conference on Multibody System Dynamics, Stuttgart, Germany, 2012*.
- [31] R. Wehage and E. J. Haug, "Generalized coordinate partitioning for dimension reduction in analysis of constrained

- dynamic systems,” *Journal of Mechanical Design*, vol. 104, pp. 247–255, 1982.
- [32] F. M. Amirouche, *Fundamentals of multibody dynamics: theory and applications*. Birkhäuser Boston, 2006.
- [33] P. Voronets, “Equations of motion for nonholonomic systems,” *Matem. Sbornik*, vol. 22, no. 4, 1901.
- [34] A. Klimchik, A. Pashkevich, and D. Chablat, “Stiffness analysis of parallel manipulator navaro with dual actuation modes,” in *2018 International Russian Automation Conference (RusAutoCon)*. IEEE, 2018, pp. 1–7.
- [35] K. Wen, T. S. Nguyen, D. Harton, T. Laliberté, and C. Gosselin, “A Backdrivable Kinematically Redundant (6+3)-Degree-of-Freedom Hybrid Parallel Robot for Intuitive Sensorless Physical Human–Robot Interaction,” *IEEE Transactions on Robotics*, 2020.
- [36] J.-F. Gauthier, J. Angeles, S. B. Nokleby, and A. Morozov, “The kinetostatic conditioning of two-limb schönfliess motion generators,” *Journal of Mechanisms and Robotics*, vol. 1, no. 1, 2009.
- [37] A. Taghvaeipour, J. Angeles, and L. Lessard, “Constraint-wrench analysis of robotic manipulators,” *Multibody System Dynamics*, vol. 29, no. 2, pp. 139–168, 2013.
- [38] O. Altuzarra, A. Zubizarreta, I. Cabanes, and C. Pinto, “Dynamics of a four degrees-of-freedom parallel manipulator with parallelogram joints,” *Mechatronics*, vol. 19, no. 8, pp. 1269–1279, 2009.
- [39] C. Germain, S. Caro, S. Briot, and P. Wenger, “Singularity-free design of the translational parallel manipulator IRSBot-2,” *Mechanism and Machine Theory*, vol. 64, pp. 262 – 285, 2013.
- [40] K. M. Lynch and F. C. Park, *Modern Robotics*. Cambridge, 2017.
- [41] R. Murray, Z. Li, and S. Sastry, *A Mathematical Introduction to Robotic Manipulation*. CRC Press, 1994.
- [42] J. Selig, *Geometric Fundamentals of Robotics*. Springer, 2005.
- [43] A. Müller, “Kinematic topology and constraints of multi-loop linkages,” *Robotica*, vol. 36, pp. 1641–1663, 2018.
- [44] A. Jain, “Graph theoretic foundations of multibody dynamics, part I: structural properties,” *Multibody Syst. Dyn.*, vol. 26, pp. 307–333, 2011.
- [45] R. W. Brockett, “Robotic manipulators and the product of exponentials formula,” *Mathematical Theory of Networks and Systems, Lecture Notes in Control and Information Sciences*, vol. 58, pp. 120–129, 1984.
- [46] A. Müller, “Screw and lie group theory in multibody dynamics –recursive algorithms and equations of motion of tree-topology systems,” *Multibody System Dynamics*, vol. 42, no. 2, pp. 219–248, 2018.
- [47] ———, “Screw and lie group theory in multibody dynamics —motion representation and recursive kinematics of tree-topology systems,” *Multibody System Dynamics*, vol. 43, no. 1, pp. 1–34, 2018.
- [48] A. Müller and S. Kumar, “Closed-form time derivatives of the equations of motion of rigid body systems,” *Multibody System Dynamics*, vol. 53, no. 3, pp. 257–273, 2021.
- [49] K. C. Gupta, “Kinematic analysis of manipulators using the zero reference position description,” *The International Journal of Robotics Research*, vol. 5, no. 2, pp. 5–13, 1986.
- [50] S. R. Ploen and F. C. Park, “Coordinate-invariant algorithms for robot dynamics,” *IEEE Transactions on Robotics and Automation*, vol. 15, no. 6, pp. 1130–1135, Dec 1999.
- [51] A. Müller, “Review of the exponential and Cayley map on SE(3) as relevant for Lie group integration of the generalized Poisson equation and flexible multibody systems,” *Proceedings of the Royal Society A: Mathematical, Physical and Engineering Sciences*, vol. 477, no. 2253, p. 20210303 (21 pages), 2021.
- [52] P. E. Nikravesh, *Computer-aided analysis of mechanical systems*. Prentice Hall, 1988.
- [53] M. Husty and P. Zsombor-Murray, “A Special Type of Singular Stewart-Gough Platform,” in *Advances in Robot Kinematics and Computational Geometry*, J. Lenarčič and B. Ravani, Eds. Springer, Dordrecht, 1994, pp. 449–458.
- [54] K. Wohlhart, “Kinematotropic linkages,” in *Recent Advances in Robot Kinematics*, J. Lenarčič and V. Parent-Castelli, Eds. Kluwer, 1996, pp. 359–368.
- [55] P. E. Nikravesh and M. Srinivasan, “Generalized co-ordinate partitioning in static equilibrium analysis of large-scale mechanical systems,” *International journal for numerical methods in engineering*, vol. 21, no. 3, pp. 451–464, 1985.
- [56] K. T. Wehage, R. A. Wehage, and B. Ravani, “Generalized coordinate partitioning for complex mechanisms based on kinematic substructuring,” *Mech. Mach. Theory*, vol. 92, pp. 464–483, 2015.
- [57] W. Blajer, W. Schiehlen, and W. Schirm, “A projective criterion to the coordinate partitioning method for multibody dynamics,” *Archive of Applied Mechanics*, vol. 64, no. 2, pp. 86–98, 1994.
- [58] Z. Terze and J. Naudet, “Structure of optimized generalized coordinates partitioned vectors for holonomic and non-holonomic systems,” *Multibody system dynamics*, vol. 24, no. 2, pp. 203–218, 2010.
- [59] W. Blajer, “Methods for constraint violation suppression in the numerical simulation of constrained multibody systems—A comparative study,” *Computer Methods in Applied Mechanics and Engineering*, vol. 200, no. 13-16, pp. 1568–1576, 2011.
- [60] A. Müller, “Dynamics modeling of topologically simple parallel manipulators: A geometric approach,” *ASME Applied Mechanics Review*, vol. 72(3), p. 27 pages, 2020.
- [61] A. Müller, “On the terminology and geometric aspects of redundant parallel manipulators,” *Robotica*, vol. 31, no. 1, p. 137–147, 2013.
- [62] X. Kong and C. M. Gosselin, *Type Synthesis of Linear Translational Parallel Manipulators*. Dordrecht: Springer

Netherlands, 2002, pp. 453–462.

- [63] Z. Huang, Q. Li, and H. Ding, *Theory of Parallel Mechanisms*. Springer Science+Business Media, 2013.
- [64] D. Gnad, H. Gattringer, A. Müller, W. Höbarth, R. Riepl, and L. Messner, “Computation of dynamic joint reaction forces of PKM and its use for load-minimizing trajectory planning,” in *IEEE International Conference on Robotics and Automation, Philadelphia, PA, June 23-27, 2022*.
- [65] F. Park, J. Bobrow, and S. Ploen, “A Lie Group Formulation of Robot Dynamics,” *The International Journal of Robotics Research*, vol. 14, no. 6, pp. 609–618, 1995.
- [66] A. Müller, “An $O(n)$ -Algorithm for the Higher-Order Kinematics and Inverse Dynamics of Serial Manipulators Using Spatial Representation of Twists,” *IEEE Robotics and Automation Letters*, vol. 6, no. 2, pp. 397–404, 2020.
- [67] M. Abdallah, A. Chen, A. Campeau-Lecours, and C. Gosselin, “How to reduce the impedance for phri: Admittance control or underactuation?” *Mechatronics*, vol. 84, p. 102768, 2022.
- [68] Alaska multibody simulation software, www.ifm-chemnitz.de/en/products/alaskamultibodydynamics, last accessed: April 23, 2022.
- [69] W. Khalil and E. Dombre, *Modeling Identification and Control of Robots*. Springer, 2004.
- [70] B. Siciliano, L. Sciavicco, L. Villani, and G. Oriolo, *Robotics: Modelling, Planning and Control*. Springer, 2009.
- [71] C. M. Gosselin and J. Angeles, “Singular analysis of closed-loop kinematic chains,” *IEEE Trans. Robotics and Automation*, vol. 6(3), pp. 281–290, 1990.
- [72] A. Müller, “Recursive second-order inverse dynamics for serial manipulators,” in *2017 IEEE International Conference on Robotics and Automation (ICRA)*. IEEE, 2017, pp. 2483–2489.
- [73] E. Haug, *Computer-Aided Kinematics and Dynamics of Mechanical Systems*. Allyn and Bacon, 1989.